Biophysical Chemistry 202 (2015) 40–57

Contents lists available at ScienceDirect

Biophysical Chemistry

journal homepage: http://www.elsevier.com/locate/biophyschem

Driving force-dependent block by internal Ba^{2+} on the Kir2.1 channel: Mechanistic insight into inward rectification

Chi-Pan Hsieh [a,b,*], Chung-Chin Kuo [c,d], Chiung-Wei Huang [c]

[a] Department of Medical Education, Far Eastern Memorial Hospital, No. 21, Nan-Ya S. Rd., Ban-Chiao, New Taipei City 220, Taiwan
[b] Department of Family Medicine, Far Eastern Memorial Hospital, No. 21, Nan-Ya S. Rd., Ban-Chiao, New Taipei City 220, Taiwan
[c] Department of Physiology, National Taiwan University College of Medicine, No. 1, Jen-Ai Road, 1st Section, Taipei, 100, Taiwan
[d] Department of Neurology, National Taiwan University Hospital, No. 7, Chung-Shan S. Road, Taipei, Taiwan

HIGHLIGHTS

- The internal Ba^{2+} block in Kir2.1 channels showed inward rectification fashion.
- The inward rectification was due to flux-dependent block.
- The steep changes in k_{on} near E_K of Ba^{2+} block is driving force-dependent.
- The high affinity Ba^{2+} binding site is located near T141.
- The single-file long cytoplasmic pore provides structural basis for flux coupling.

GRAPHICAL ABSTRACT

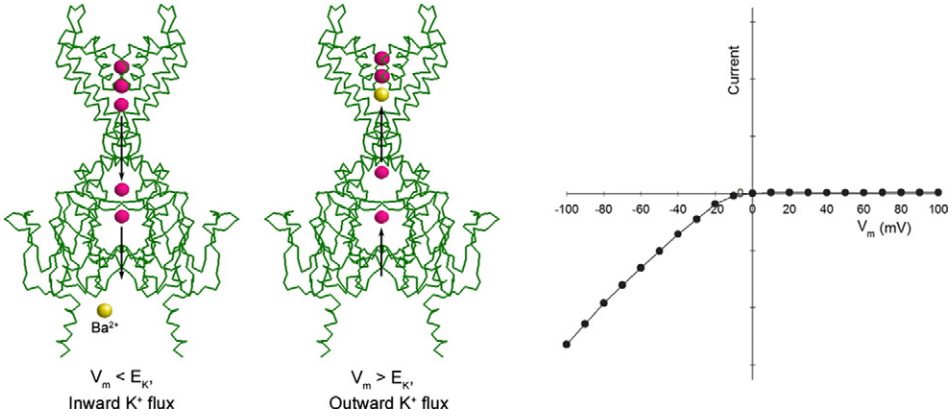

ARTICLE INFO

Article history:
Received 31 March 2015
Received in revised form 6 April 2015
Accepted 6 April 2015
Available online 15 April 2015

Keywords:
Kir2.1 channel
Inward rectification
Ba^{2+} block
Flux-coupling effect

ABSTRACT

The Kir2.1 channel is characterized by strong inward rectification; however, the mechanism of the steep voltage dependence near the equilibrium potential remains to be investigated. Here, we studied the internal Ba^{2+} block of the Kir2.1 channel expressed in *Xenopus* oocytes. We showed that the driving force and thus the K^+ ion flux significantly influenced the apparent affinity of the block by internal Ba^{2+}. Kinetic analysis revealed that the binding rate shifted with the driving force and changed steeply near the equilibrium point, either in the presence or absence of the transmembrane electrical field. The unbinding rate was determined by the intrinsic affinity of the site. Mutagenesis studies revealed that the high-affinity binding site for Ba^{2+} was located near T141 at the internal entrance of the selectivity filter. The steep change of the blocking affinity near the equilibrium potential may result from the flux-coupling effect in the single-file, multi-ion cytoplasmic pore.

1. Introduction

Inward rectifier K^+ channels (Kir channels) are a family of K^+ channels composed of four subunits with two transmembrane segments (2TM). Kir channels play important physiological roles. For example, Kir2.1 channels can regulate the resting membrane potential and

* Corresponding author at: Department of Medical Education, Department of Family Medicine, Far Eastern Memorial Hospital, No. 21, Nan-Ya S. Rd., Ban-Chiao, New Taipei City 220, Taiwan. Tel.: +886 9 20178473.
E-mail address: hsiehcp@ntu.edu.tw (C.-P. Hsieh).

http://dx.doi.org/10.1016/j.bpc.2015.04.003
0301-4622/

shape electrical signals in the heart and in neurons. K_{ATP} channels can control insulin secretion in the pancreas in response to glucose level. Kir1.1 channels in the kidney are involved in the maintenance of electrolyte balance [1].

Some Kir channel family members, e.g., the Kir2.1 channel, are characterized by strong inward rectification in their current–voltage relations. When the membrane potential (V_m) is negative relative to the equilibrium potential (E_K), the inward K^+ currents are much larger than the outward K^+ currents at voltages positive to E_K [1–3]. The strong inward rectification has been attributed to the blockage of outward currents by intracellular Mg^{2+} [4,5] and polyamines [6,7]. The outward currents are very sensitive to the intracellular blockers, whereas the inward currents are relatively unaffected. The inhibition of the outward currents by intracellular blockers has been shown to be dependent on the driving force ($V_m - E_K$) for the K^+ ion flux. When V_m is smaller than E_K, the apparent sensitivity of the inward currents to the blocker is very small; however, the extent of the blockage increases steeply when the membrane potential becomes positive to E_K. If the E_K is shifted by changing the extracellular or intracellular K^+ concentration, the current–voltage ($I–V_m$) curve in the presence of the blocker will shift in parallel with the E_K.

The physical mechanism underlying the steep voltage dependence of the $I–V_m$ curve near E_K is still controversial, and the molecular events underlying the phenomenon remain a subject worthy of study. The Woodhull view of voltage-dependent channel block [8], which assumes independent movements between the conducting ions and the blocker, is insufficient to explain the steep voltage dependence of Kir channels. The voltage dependence of the apparent affinities of internal tetraethylammonium (TEA) or Mg^{2+} is much larger than what can be attributed to the fraction of the electrical field traversed by the positively charged blocking ions. The measured voltage dependence values, $z\delta$, were shown to be nearly identical for monovalent TEA and for divalent Mg^{2+} in Kir1.1 channels [9]. In a study of the block of Kir2.1 channels by polyamines, spermine (4+) and spermidine (3+) had similar apparent voltage dependence near E_K [10]. Coupling between the K^+ ions and the blocking ion in the long channel pore seemed to be a crucial component of the mechanism of inward rectification. However, how the ion-flux coupling relates to the inward rectification remains to be investigated.

The scenario underlying the inward rectification in Kir channels may be more complicated than simple pore blockage. Both high-affinity and low-affinity blocks contribute significantly to the $I–V_m$ relationship in Kir channels [11,12]. The high-affinity spermidine block may not completely occlude the single-channel pore, but rather elicit a subconducting state [12]. Moreover, neutralization of the ring of charges near E224, either by mutagenesis or by the binding of cationic blockers, may induce some intrinsic gating mechanism that contributes to inward rectification [13–15].

To focus on the detailed mechanism of pore blockage by the internal cation and to study the contribution of flux-coupling effects to the inward rectification in the multi-ion long pore, in this study, we investigated the interaction between intracellular Ba^{2+} ions and cloned mouse Kir2.1 channels expressed in *Xenopus* oocytes. We examined the effects of intracellular Ba^{2+} on the macroscopic Kir2.1 currents using patch-clamp recording techniques. The Ba^{2+} ion has been shown to be useful as a probing pore blocker of Kir2.1 channels and of calcium-activated K^+ channels [13,16–21]. The Ba^{2+} ion (1.35 Å) and the K^+ ion (1.33 Å) have a similar Pauling radius. The dehydrated Ba^{2+} ion may bind to some K^+-ion binding sites in the K^+ channel pore, enabling Ba^{2+} to serve as a pore blocker that completely occludes the K^+ channel pore. Though the Ba^{2+} ion is not an endogenous blocker of Kir channels in physiological conditions, the discrete blocking kinetics of Ba^{2+} with K^+ channels facilitate the study of the detailed kinetics of pore block. The majority of the studies previously conducted on Kir channels examined the effect of extracellular Ba^{2+} on inward currents. Only one study by Shieh et al. [20] examined the interaction of internal Ba^{2+} with Kir2.1 channels. Study of the mechanism of the blockage by intracellular Ba^{2+} would be important and interesting because the internal Ba^{2+} block of Kir2.1 channels also has the feature of inward rectification. By studying the kinetics of intracellular Ba^{2+} blockage, we tried to elucidate the mechanism of inward rectification by distinguishing between the contribution of binding and unbinding processes to the steep voltage dependence near E_K. We showed that the steep voltage dependence of the block of outward currents by internal Ba^{2+} results from the flux-coupling effect. Coupling between the K^+ ion flux and the Ba^{2+} in the cytoplasmic long pore of Kir2.1 channels significantly affected the apparent affinity, mainly through an effect on the binding rate between internal Ba^{2+} and Kir2.1 channels. The single-file, multi-ion cytoplasmic pore, a structural feature of Kir channels [22–26], is essential for the flux-dependent block and the resultant inward rectification.

2. Materials and methods

2.1. Molecular biology and Xenopus oocyte preparation

Mouse Kir2.1 channels (UniProt: P35561) [14] were expressed on the cell membrane of *Xenopus* oocytes for patch-clamp recordings. Wild-type Kir2.1 cDNA (GenBank X73052) subcloned into Bluescript II SK+ was kindly shared by Dr. Ru-Chi Shieh (Institute of Biomedical Sciences, Academia Sinica, Taiwan). Mutant channel cDNAs were prepared using the QuikChange site-directed mutagenesis kit (Stratagene, La Jolla, CA, USA). All mutations were confirmed by DNA sequencing. RNA was synthesized in vitro using the T7 mMESSAGE mMACHINE transcription kit (Ambion, Austin, TX, USA) from Not I-linearized cDNAs.

Xenopus oocytes were obtained surgically from mature female *Xenopus laevis* frogs under the guidance of the National Taiwan University College of Medicine and College of Public Health Institutional Animal Care and Use Committee. The oocytes were agitated on a platform shaker at 80–100 rpm for 60–90 min in a solution containing (in mM): 82.5 NaCl, 2 KCl, 1 $MgCl_2$, 5 HEPES, and 2 mg/ml collagenase (from *Clostridium histolyticum*, type I), pH = 7.6. The defolliculated stage IV and stage V oocytes were selected and incubated in ND96 solution containing (in mM): 96 NaCl, 2 KCl, 1.8 $CaCl_2$, 1 $MgCl_2$, 5 HEPES, and 50 μg/ml gentamycin, pH = 7.6 at 18 °C. RNAs were injected into the oocytes 16–72 h before electrophysiological recordings.

2.2. Electrophysiological recordings and solutions

Cell-attached and inside-out patch-clamp recordings were performed on the oocytes expressing the wild-type and mutant Kir2.1 channels at room temperature (22–25 °C). Voltage-clamp recordings were made with the Clampex 6.0 portion of pClamp software, (Axon Instruments, Foster City, CA, USA) using an Axoclamp 200A amplifier. Data were low-pass filtered to 1–2 kHz and digitized at 1–10 kHz through a Digidata-1200 analog/digital interface. The oocyte was put in a recording chamber in a bath solution containing (in mM): 82 KCl + KOH, 5 EDTA, 8 K_2HPO_4, and 2 KH_2PO_4, pH = 7.4 (100 mM K^+). Some experiments were carried out using HEPES-buffered solutions. The vitelline membrane of the oocyte was removed in the bath solution using forceps. Pipettes were pulled from borosilicate glass and polished. The pipette solution (external solution) and the control internal solution were the same as the bath solution. In the experiments in which the K^+ concentration of solutions differed from 100 mM, the desired K^+ concentrations were obtained by adjusting the content of KCl and KOH. The pipette resistance was 100–400 kΩ when the pipette was filled with the 100 mM K^+ pipette solution. For inside-out recordings, the patch was pulled from the membrane of the oocyte after the cell-attached configuration was obtained. The patch was lifted and moved to the mouth of one of the gravity-driven flow pipes that emitted various internal solutions to the cytoplasmic side of

the patch. Rapid changes of the internal solutions were achieved by a stepper motor (SF-77B perfusion system, Warner Instrument).

To slow the run-down of the Kir2.1 currents in the inside-out configuration, once the inside-out configuration was obtained, the patches were initially treated with 20 μM phosphatidylinositol-4,5-bisphosphate (PIP_2) in modified FVPP solution containing (in mM): 64 KCl, 16 K_2HPO_4, 4 KH_2PO_4, 5 EDTA, 5 NaF, 0.1 Na_3VO_4, and 10 $Na_4P_2O_7$, pH = 7.4 from the cytoplasmic side for 30–60 s [20,27,28]. Alternatively, a MgATP solution containing (in mM) 85 KCl, 2 MgATP, 5 K_2HPO_4, and 5 KH_2PO_4, pH = 7.2 with KOH was used to slow the run-down or to reactivate the channels [29].

In Ba^{2+}-block studies, free Ba^{2+} concentrations were estimated according to temperature, pH, and ionic strength using the software WinMaxc 32 v.2.50 (http://maxchelator.stanford.edu). When the free Ba^{2+} concentration is 30 μM or above, the endogenous divalent-activated Cl^- currents of the oocytes would be activated. To avoid the interference of these Cl^- currents, methanesulfonate was used to replace Cl^- in the internal and external solutions, except that 5 mM Cl^- was left in the pipette solution for proper ionic conduction. Niflumic acid (500 μM) was added to the internal solution to inhibit the Cl^- currents [30,31]. The Ba^{2+} solution was prepared from $Ba(OH)_2$. All chemicals were from Sigma.

Data were analyzed with Clampfit 8.0 (Axon Instruments), Excel 2000 (Microsoft, Redmund, WA, USA), and SigmaPlot 6.0 (SPSS, Chicago, IL, USA). The results are given as the mean ± standard error of the mean.

3. Results

3.1. The Kir2.1 channel currents showed strong inward rectification in cell-attached recordings

Macroscopic Kir2.1 channel currents were recorded from *Xenopus* oocytes using the patch-clamp recording technique. In the cell-attached configuration, strong inward rectification was observed, as in previous studies [4,5,7]. The outward currents were blocked by endogenous positively charged blockers such as Mg^{2+} and polyamines; the inward currents were relatively unaffected. The current–voltage curve had a steep deflection near the equilibrium potential of the K^+ ion flux in the cell-attached configuration (Fig. 1). In the inside-out

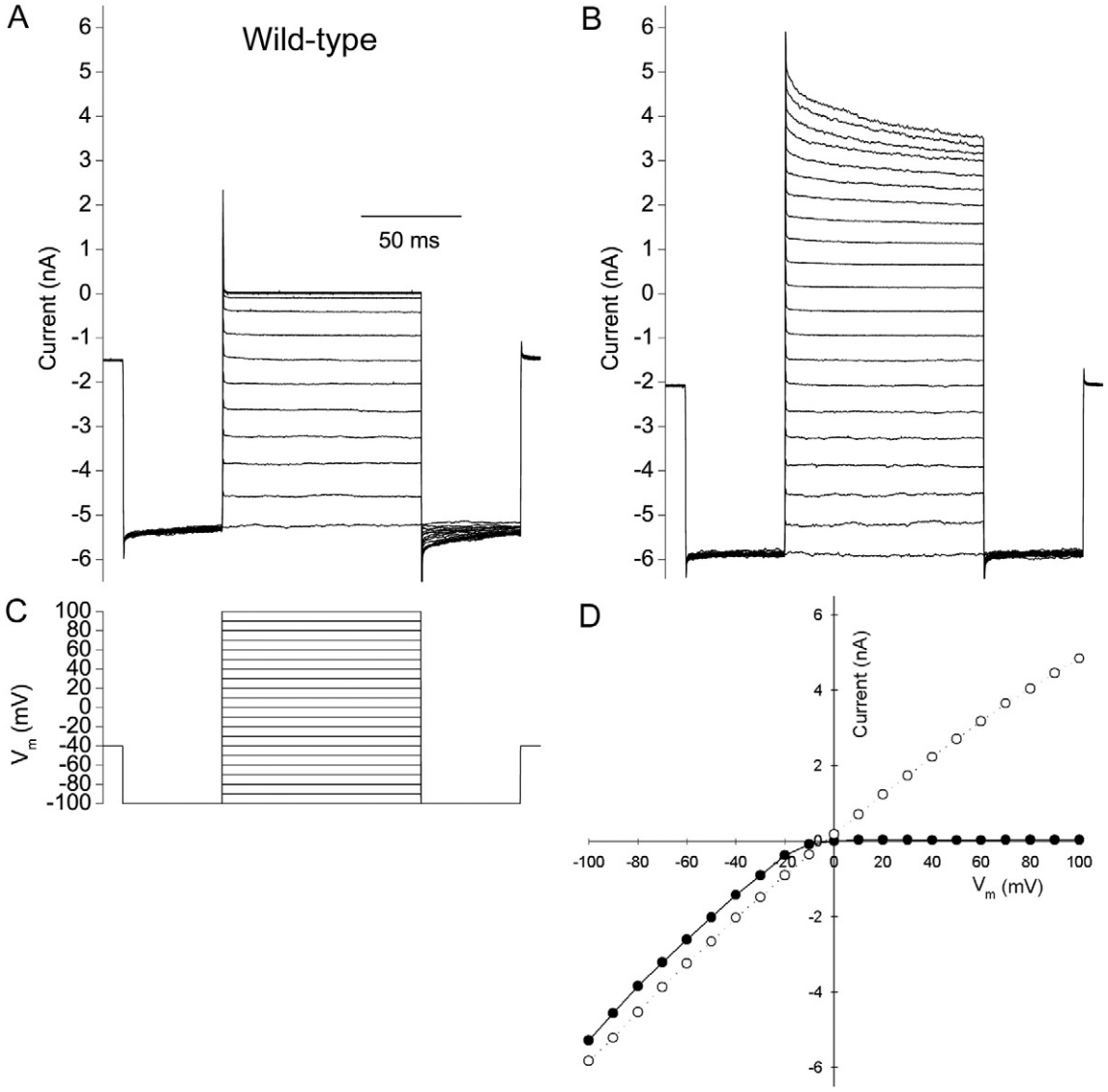

Fig. 1. I–V_m relations of the wild-type Kir2.1 channel in (A) cell-attached configuration and (B) inside-out configuration when the external and internal K^+ concentrations were both 100 mM. (C) The voltage stimulus protocol. The test voltages were stepped from −100 mV to 100 mV in 10-mV increments every 300 ms. (D) The instantaneous I–V_m curves of the inside-out (open circle) and cell-attached (closed circle) configurations.

configuration, when the patches were washed from the cytoplasmic side with the blocker-free control solution, the instantaneous I–V_m relation became nearly linear. The outward currents of the wild-type Kir2.1 decayed with time to various degrees at voltages positive to +40 mV, despite washing in the phosphate-buffered control solution for more than 20 min. The decay may be due to the block of trace amounts of contaminating blockers [32] and to some intrinsic gating mechanism of the channel [33]. All experiments described below were carried out using inside-out recordings from the patches when the endogenous blockers were washed out to a steady state, typically more than 5 min after being washed by the control solution.

3.2. Internal Ba^{2+} inhibited the currents in an inward-rectifying manner and dissociated very slowly during repolarization

Internal Ba^{2+} block of wild-type Kir2.1 channel currents was examined under conditions of $[K^+]_{out} = 100$ mM and $[K^+]_{in} = 100$ mM ($E_K = 0$ mV). Currents were inhibited by internal Ba^{2+} (0.1 μM to 10 μM) in an inward-rectifying manner, as described previously [20]; the outward currents were inhibited by internal Ba^{2+}, and the inward currents were relatively much more resistant to the internal Ba^{2+} block (Fig. 2). The rate of Ba^{2+}-mediated inhibition increased markedly with voltage from +10 mV to +40 mV. We analyzed the inhibition rates by subtracting the current traces in the presence of Ba^{2+} ions from the currents in control solutions and fitting the resultant current trace using a single exponential. In 1 μM Ba^{2+}, the τ values were 214 ± 0.05 ms ($n = 8$) at +20 mV, 7.75 ± 0.04 ms ($n = 9$) at +40 mV, and 3.71 ± 0.05 ms ($n = 9$) at +60 mV (Fig. 2B). The dose dependence of the internal Ba^{2+}-mediated inhibition of the outward current by is shown in Fig. 2D. To obtain the apparent dissociation constant (K_d) of the Ba^{2+} block, the relative currents were plotted against the $[Ba^{2+}]$, and the data were fit using the Langmuir equation for one-to-one binding, $f = 1 / (1 + [Ba^{2+}] / K_d)$, where f is the relative current. The apparent dissociation constants decreased steeply from +10 mV to +40 mV (Fig. 2E). The K_d values then reached more steady values when the test voltages were above +50 mV and even increased slightly with voltage at voltages above +70 mV. The voltage dependence of K_d from +10 mV to +40 mV was obtained by fitting the data at the various test voltages (V_m) using the equation:

$$K_d(V_m) = K_d(0)\exp\left(\frac{z\delta F V_m}{RT}\right) = K_d(0)\exp\left(\frac{z\delta V_m}{25\ \text{mV}}\right). \quad (1)$$

Here, F, R, and T have their usual thermodynamic meanings. The fit results were $K_d(0) = 49 \pm 3.9$ μM and $z\delta = -3.34 \pm 0.18$. The steep voltage dependence found here needs cautious interpretation. In the

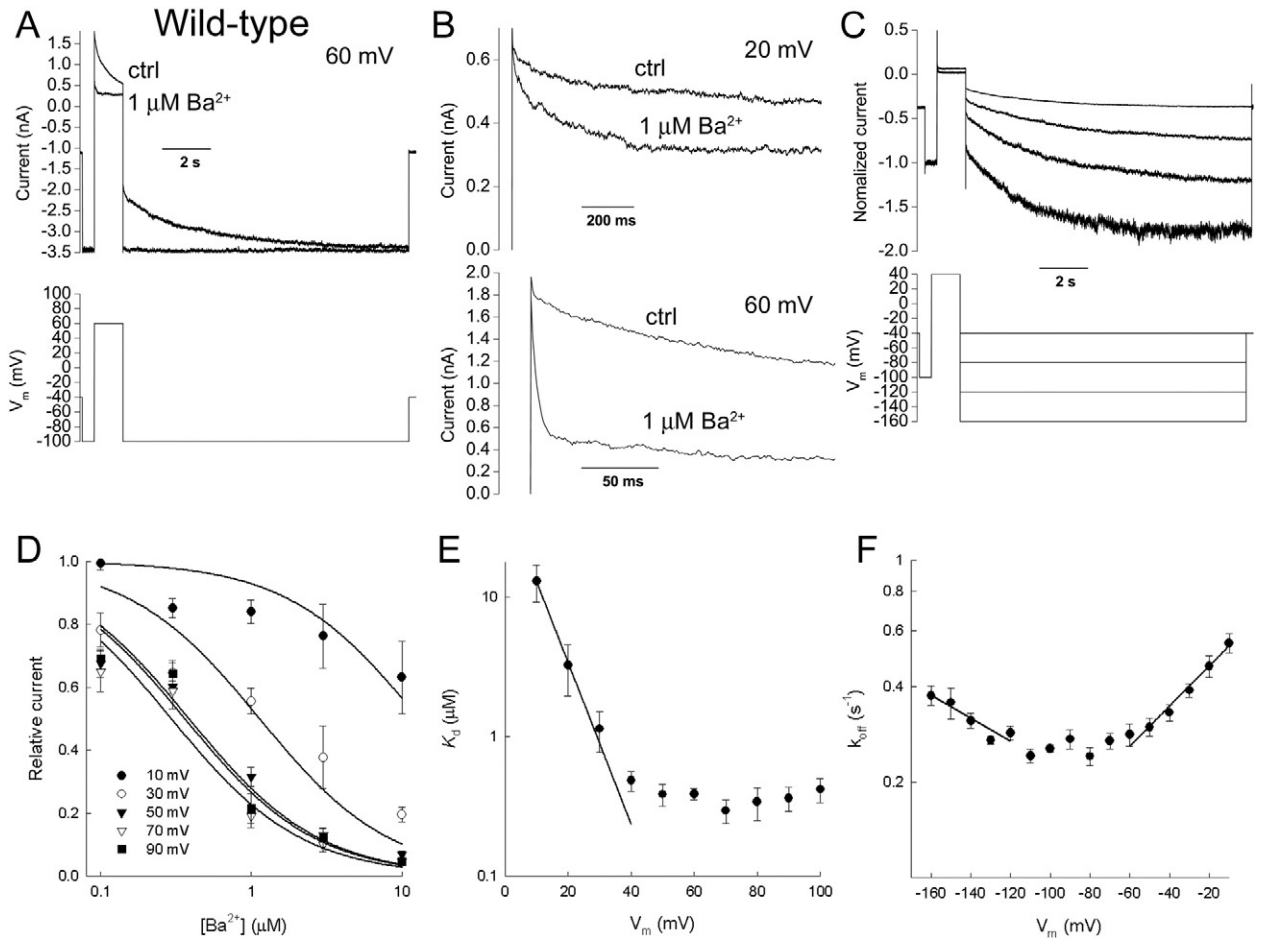

Fig. 2. Internal Ba^{2+} block of outward Kir2.1 currents in an inward-rectifying manner and dissociated very slowly during repolarization. (A) Ba^{2+} (1 μM) inhibited 70% of the outward current at +60 mV and spared the inward currents from blockage in $[K^+]_{out} = 100$ mM and $[K^+]_{in} = 100$ mM. (B) Representative currents in control and in 1 μM Ba^{2+} at test voltages of +20 mV and +60 mV. (C) The recovery rates were slow upon repolarization. The outward currents were inhibited by 10 μM internal Ba^{2+} at the test voltage of +40 mV, and then the voltage was stepped to −10 mV to −160 mV. The long tails were fit with a single exponential. (D) Dose-dependent inhibition by 0.1 μM, 0.3 μM, 1 μM, 3 μM, and 10 μM internal Ba^{2+}. The relative currents were the steady-state fractional currents in the Ba^{2+} solutions relative to the currents in the control solutions. The lines were fit using the Langmuir equation for one-to-one binding. (E) The apparent dissociation constant, K_d, (in log scale) was plotted against test voltage, V_m. The K_d from +10 mV to +40 mV was fit using Eq. (1). The line was fit with $K_d(0) = 49 \pm 3.9$ μM and $z\delta = 3.34 \pm 0.18$ ($n = 3$–10). (F) The dissociation rate of the long recovery tails in (C), k_{off} (log scale), was plotted against the voltage. From −160 mV to −120 mV, k_{off} values decrease with voltage. The line was fit using Eq. (2): $k_{off}(0) = 0.10 \pm 0.02\ s^{-1}$ and $z\delta = 0.21 \pm 0.04$. k_{off} values from −60 mV to −10 mV increase with voltage. The line is the fit with $k_{off}(0) = 0.62 \pm 0.02\ s^{-1}$ and $z\delta = -0.37 \pm 0.03$ ($n = 4$–6).

study of voltage-dependent block, Eq. (1) is usually used to estimate the equivalent electric distance of the binding site under the rationale that the blocker with valence z binds to the site located at the equivalent electric distance δ within the transmembrane electric field [8], under the assumption that the binding process of the blocker is independent of the conducting ions. If Ba^{2+} block is significantly coupled to the K^+ ion flux and δ can be larger than 1, then $z\delta$ cannot be interpreted as the potential energy difference [9,34]. Though here, we fit the dose- and voltage-dependent internal Ba^{2+}-mediated inhibition of Kir2.1 currents using the conventional one-to-one binding formula, the actual mechanism of Ba^{2+} inhibition may be more complex in several aspects. A large $z\delta$ value indicates ion-flux coupling between the conducting K^+ ions and the Ba^{2+} ion in the narrow and long channel pore. A shallower low-affinity binding site (with a much faster k_{off}) may coexist with a deeper high-affinity binding site (with a slow k_{off}) in Kir channels [11,12], so the one-to-one assumption may not be valid. Further, the internal Ba^{2+}-mediated inhibition may be related to cation-induced gating in addition to pore block [13,20].

We found that the recovery phase of the Ba^{2+} block was very slow during repolarization when the voltage was stepped back to −100 mV from the test pulse (Fig. 2A), a finding that has not been reported previously, The time constant, τ, was ~ 4 s at −100 mV when the long recovery tail current was fit using a single exponential, which contrasts with the rapid recovery rate (within milliseconds) of the block by Mg^{2+} and polyamines shown in Fig. 1. The slow recovery suggests that internal Ba^{2+} ions may reach and bind to a high-affinity binding site during the test pulse and may dissociate very slowly from this binding sites at negative voltages ($k_{off} = 1/\tau = 0.25$/s at −100 mV). It is interesting that Kir2.1 channels can exhibit strong inward rectification during internal Ba^{2+} blockage despite the fact that the dissociation rate from the Ba^{2+} binding site is also very slow at negative voltages. The slow unbinding rate raises key questions about the mechanism of the inward rectification in internal Ba^{2+} block: how does the direction of K^+ ion flux affect the apparent affinity of the internal blockers? Is the binding rate or the unbinding rate affected by K^+ ion flux and can thus determine the phenomenon of inward rectification? If the low affinity of the blocker at negative voltages were due to constant, rapid push-off of the blocker from the binding site by the inward K^+ ion flux [35], the unbinding rate at negative voltages might have been very fast. However, as shown in Fig. 2A, the unbinding rate of Ba^{2+} is too slow to account for the low sensitivity of the inward currents to internal Ba^{2+} when the voltage was steadily held at −100 mV. A plausible mechanism for the low sensitivity of the inward K^+ currents is that when the K^+ ion flux is steadily inward, the Ba^{2+} ions in the internal solution can have difficulty binding to the high-affinity binding site because the permeation route to the binding site is hindered by the inward K^+ flux, which means that there may be at least one K^+ binding site internal to the Ba^{2+} binding site along the narrow channel pore.

3.3. The voltage dependence of the slow dissociation rate implies that Ba^{2+} may exit to the external side as well as to the internal side through the Kir channel pore

We further analyzed the voltage dependence of the recovery rates by stepping the voltages to −10 mV to −160 mV from a test pulse at +40 mV (Fig. 2C). The long tails were fit using a single exponential with a time constant (τ), and the unbinding rate (k_{off}) of Ba^{2+} from the high-affinity binding site can be estimated from the relation: $k_{off} = 1/\tau$. Fig. 2F shows the values and the voltage dependence of k_{off}. From −160 mV to −120 mV, k_{off} values decreased as the voltage increased and were fit using:

$$k_{off} = k_{off}(0)\exp\left(\frac{z\delta V_m}{25\ \text{mV}}\right). \quad (2)$$

The fit results were as follows: $k_{off}(0) = 0.10 \pm 0.02\ s^{-1}$ and $z\delta = -0.21 \pm 0.04$. k_{off} values were the smallest from approximately −100 mV to −80 mV and then increased with voltage from −80 mV to −10 mV. The fits for k_{off} from −60 mV to −10 mV using Eq. (2) were $k_{off}(0) = 0.62 \pm 0.02\ s^{-1}$ and $z\delta = 0.37 \pm 0.03$. The results suggest that in the experimental ionic conditions ($[K^+]_{out} = 100$ mM and $[K^+]_{in} = 100$ mM), Ba^{2+} from the internal solution may reach and bind to a high-affinity binding site when the test voltage is positive to E_K; then, the Ba^{2+} may either return to the internal side or exit to the external side of the Kir channel. Ba^{2+} ions may dissociate and return to the intracellular solution when the voltage is stepped back to voltages negative to −120 mV or may dissociate and traverse the selectivity filter to the extracellular solution when the voltage is stepped back to voltages positive to −80 mV. At voltages between −120 mV and −80 mV, the Ba^{2+} ion dissociates and exits to either the external side or to the internal side, with comparable probabilities. The measured unbinding rate is the sum of the unbinding rate into the extracellular solution and the unbinding rate into the intracellular solution. The idea that Ba^{2+} can cross through a K^+ channel pore has been reported previously in blocking kinetics studies of the high-conductance Ca^{2+}-activated K^+ channel [19].

The voltage dependence of the slow dissociation rates in Kir2.1 channels at voltages negative to the equilibrium potential ($E_K = 0$ mV in the experimental conditions, Fig. 2F), indicates that the unbinding process of Ba^{2+} is not strongly influenced by the direction of the K^+ ion flux. The direction of Ba^{2+} exit changes at voltages from approximately −100 mV to −80 mV but not at the equilibrium potential of K^+ ion currents. At voltages from −80 mV to −20 mV, most Ba^{2+} ions dissociate and exit to the external solution even when net K^+ ion flux is predominantly inward, and the dissociation rate, k_{off}, increases as the voltage becomes more positive. Hence, the "rapid push-off" model [35] cannot explain the low affinity of internal Ba^{2+} block when K^+ ion flux is predominantly inward. The exit direction of the Ba^{2+} ions from the high-affinity binding sites seems to be determined mainly by the intrinsic internal and external energy barriers of the high-affinity Ba^{2+} binding site rather than by the direction of the conducting K^+ ion flux.

3.4. Kinetic studies of E224G mutant Kir2.1 channels reveal that the strong inward rectification of internal Ba^{2+} block results from a change in the apparent binding rate near E_K

Because the apparent dissociation constant $K_d = k_{off}/k_{on}$, it seems logical that we could analyze the kinetics of the inhibition and find out whether the steep voltage dependence of K_d near E_K results from a steep increase in k_{on} or from a steep drop in k_{off}. However, in wild-type Kir2.1 channels, there are theoretical and experimental factors that confound the analysis. First, at least two binding events are involved in the internal Ba^{2+}-mediated block of the outward currents. The shallower low-affinity binding site (with a much faster k_{off}) and the deeper high-affinity binding site (with a slow k_{off}) coexist [11,12]; therefore, the one-to-one binding analysis may not be valid. Second, the outward currents of wild-type Kir2.1 decayed with time to various degrees at voltages positive to +40 mV despite washing with the phosphate-buffered control solution for more than 20 min. The decay may be due to the block of trace amounts of contaminating blockers [32] or may involve some intrinsic gating mechanism of the channel [33]. Third, the fast component of the internal Ba^{2+}-mediated inhibition may be related to cation-induced gating in addition to pore block [13,20]. However, we will show below that in the E224G mutant, kinetic analysis of one-to-one pore block becomes feasible. The E224 residue is located in the cytoplasmic pore (Fig. 9C). In the E224G mutant, in which the ring of charges of E224 in the cytoplasmic pore region was neutralized by mutagenesis, the internal Ba^{2+}-mediated inhibition of outward currents can be explained by one-to-one binding. Because the E224 residue has been neutralized, the faster events caused by the shallower

low-affinity block or by the cation-induced gating would no longer interfere with the Ba^{2+}-mediated block of the pore via the high-affinity binding site, which we want to investigate. This idea is compatible with polyamine block studies that showed that the E224G mutation in the cytoplasmic pore region reduced sensitivity to the low-affinity block without markedly altering sensitivity to the high-affinity block [11]. Additionally, the outward currents of the E224G mutant were stationary at positive voltages and did not decay with time during the test pulses. Hence, we performed most of the kinetic analysis in the E224G mutant.

The I–V_m relations of E224G in the inside-out recording are shown in Fig. S1. There is an intrinsic inward rectification in the absence of the blocking ions in E224G due to the neutralization of the negative charges of the glutamate residues [13,15,36]. The magnitude of the instantaneous outward current at +100 mV is approximately 45% of the current at −100 mV. Internal Ba^{2+} block of the outward currents of the E224G mutant is shown in Fig. 3A. At +60 mV, the steady-state fractional current at the end of the 1.2 s test pulse was 0.30 ± 0.03 in 10 μM internal Ba^{2+}, and when the voltage was stepped back to −100 mV, the initial fraction of the recovered current (the ratio of the head of the long tail to the steady-state current at −100 mV) was also 0.30. At test voltages from +10 mV to +100 mV, the steady-state fractional currents were all similar to the initial recovery ratios at −100 mV (not shown). The result support the hypothesis that the internal Ba^{2+} block in E224G mutant channels is a one-to-one binding event and the idea that almost all the inhibition of the outward current is due to the Ba^{2+}-mediated block of the pore via the high-affinity site. The blocking rates could be obtained by fitting with a single exponential. The time constant of the long tail during recovery when the voltage was stepped back to −100 mV was the same as that in the wild-type channel, which suggests that the high-affinity Ba^{2+} binding site is not affected by the mutation. The dose dependence and the voltage dependence of the internal Ba^{2+} block are shown in Fig. 3D and E. The dose dependence of the block by internal Ba^{2+} in E224G reveals that the voltage dependence of the block is steep at +10 mV to +40 mV in symmetric 100 mM K^+ solutions. The K_d values decreased with voltage from +10 mV to +30 mV, with $z\delta = -3.58 \pm 0.78$ and $K_d(0) = 116 \pm 39$ μM. The extent of the block was maximal at +40 mV, and the fractional current unblocked increased with voltage from +50 mV to +100 mV. At +60 mV to + 100 mV, $K_d(0) = 2.34 \pm 1.74$ μM and $z\delta = 0.33 \pm 0.22$.

To clarify the mechanism of the inward rectification of the Kir2.1 channel induced by the pore block by internal Ba^{2+}, we wanted to

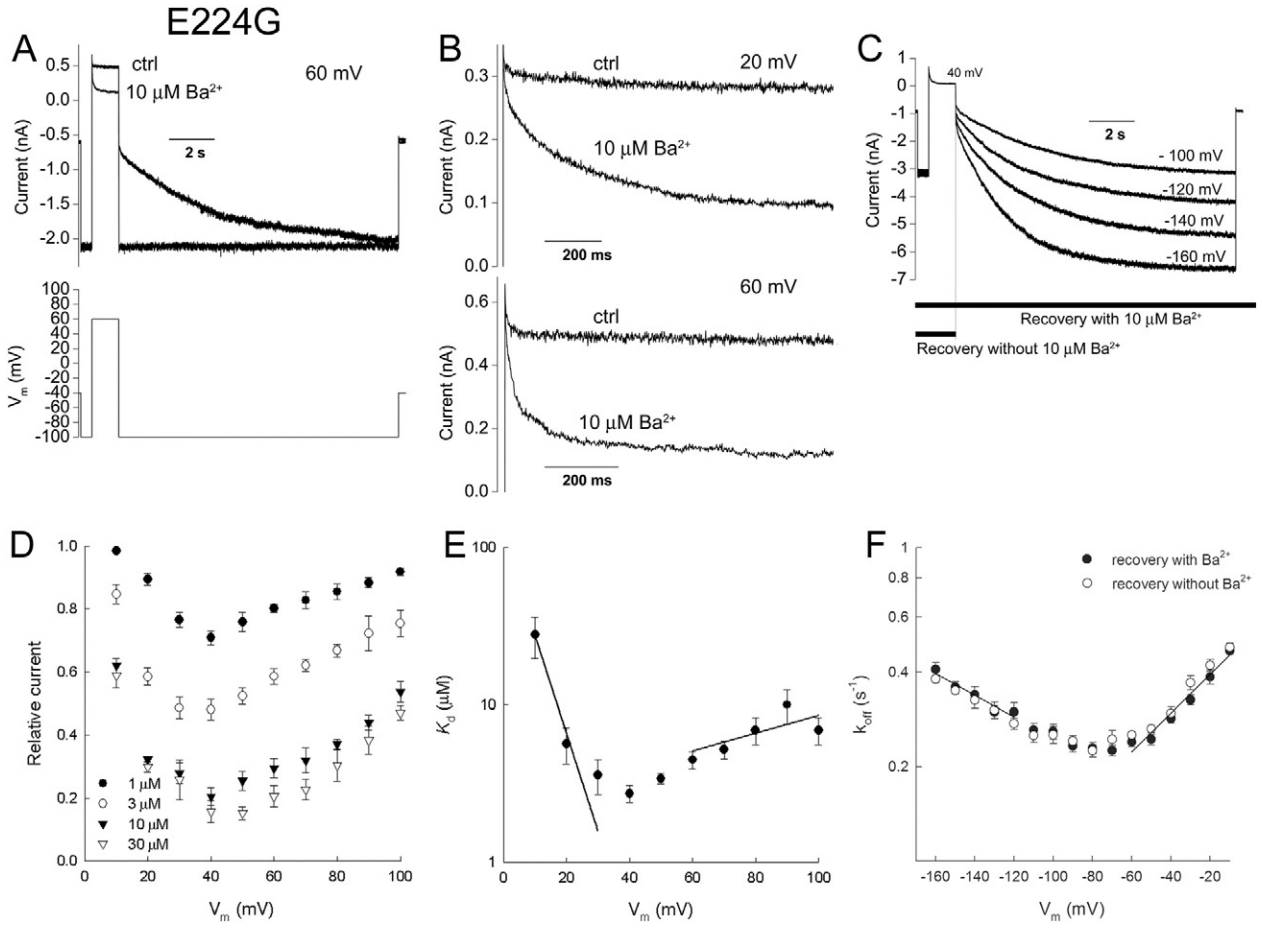

Fig. 3. Internal Ba^{2+} block of the outward currents of the E224G mutant in inside-out recordings in $[K^+]_{out} = 100$ mM and $[K^+]_{in} = 100$ mM. (A) The outward current at +60 mV was blocked by an internal concentration of 10 μM Ba^{2+}. (B) Representative currents in control and in 10 μM Ba^{2+} at test voltages of +20 mV and +60 mV. The control current decays little with time, and the blocking rates were measured from the currents in Ba^{2+}. The value of τ is 282 ± 14 ms at +20 mV and 59 ± 3.6 ms at +60 mV. (C) The dissociation rates when the voltage is repolarized to different voltages from the block by 10 μM internal Ba^{2+} at +40 mV in E224G. In one group, the internal Ba^{2+} was present during the whole process, including the recovery period, from −10 mV to −160 mV; in the other group, the internal solution was changed to the control solution without Ba^{2+} during the recovery period using the rapid stepper motor. (D) Dose dependence and the voltage dependence of the block by 1 μM, 3 μM, 10 μM, and 30 μM Ba^{2+}. (E) The estimated K_d values are plotted against the voltage. The K_d values decrease steeply with voltage from +10 mV to +40 mV and increase with voltage from + 50 mV to + 100 mV. The straight line is the fit using a single exponential. At +10 mV to + 30 mV, $K_d(0) = 116 \pm 39$ μM and $z\delta = 3.58 \pm 0.78$. At +60 mV to +100 mV, $K_d(0) = 2.34 \pm 1.74$ μM and $z\delta = -0.33 \pm 0.22$ (n = 4–10). (F) The k_{off} values of the long recovery tails in (C) with and without Ba^{2+} are nearly the same during the recovery period. The fit using a single exponential was performed in the Ba^{2+}-present group. At −160 mV to −120 mV, $k_{off}(0) = 0.10 \pm 0.02$ s^{-1} and $z\delta = -0.21 \pm 0.03$. At −60 mV to −10 mV, $k_{off}(0) = 0.53 \pm 0.02$ s^{-1} and $z\delta = 0.37 \pm 0.03$ (n = 6–10).

analyze the kinetic rate constants and determine whether the steep voltage dependence of K_d near E_K results from k_{on} or k_{off}. As aforementioned, to focus on the pore-block mechanism of Ba^{2+} binding with the high-affinity site and to avoid the interference of the unknown fast inhibition, we carried out the following experiments in the E224G mutant channel. In E224G, the inhibition of the outward currents is almost exclusively due to the pore block by the Ba^{2+} ion via the high-affinity site.

The blocking kinetics were analyzed using the following relations, with the assumption that the block was one-to-one binding [20,37].

$$k_{on} = \frac{1-f}{\tau\ [Ba^{2+}]} \tag{3}$$

$$k_{off} = \frac{f}{\tau}. \tag{4}$$

Here, f is the relative current, that is, the ratio of the steady-state current in the Ba^{2+} solution to the steady-state current in the control solution. The voltage dependence of the k_{on} and k_{off} values could be fit using Eq. (5) and Eq. (2)

$$k_{on} = k_{on}(0)\exp\left(\frac{z\delta V_m}{25\ mV}\right). \tag{5}$$

Interestingly, as shown in Fig. 4, the k_{on} values increased steeply with voltage at +10 mV to +40 mV ($z\delta = 2.62 \pm 0.61$ from +10 mV to +30 mV) and then reached more steady values with milder voltage dependence at +50 mV to +100 mV ($z\delta = 0.11 \pm 0.10$ from +60 mV to +100 mV). In contrast, the k_{off} values increased monotonically over +10 mV to +100 mV, with $z\delta = 0.78 \pm 0.05$. The results of the kinetic analysis have important significance. The steep voltage dependence of K_d from +10 mV to +40 mV results from the steep increase of k_{on} over the same range of V_m. As we know, the apparent binding rate constant k_{on} is determined by two factors: the encounter frequency between the blocker and the binding site and the activation barrier of the binding reaction. The encounter frequency has an upper limit set by the rate of diffusion of molecules in solution. In the present case, the encounter frequency of Ba^{2+} and the high-affinity binding site may be significantly affected by the K^+ ion flux. The flux-coupling effect influences the probability that the blocking ion will encounter the binding site. When the K^+ flux is inward, the Ba^{2+} has little access to the binding site because the inward-flowing K^+ ions hinder the pathway to the binding site. When the K^+ flux is outward, the Ba^{2+} is coupled with the outward K^+ flow and can reach the binding site. The steep voltage dependence of k_{on} from +10 mV to +40 mV may result from the change in driving force near E_K and thus also from the steep increase in the outward K^+ flux and the flux-dependent encounter frequency between Ba^{2+} and the binding site. The effect of flux coupling on the increase of the apparent binding rate seems to saturate at voltages positive to +40 mV. At voltages positive to +40 mV, the apparent binding rate may be limited by the activation barrier of the Ba^{2+} binding reaction because the flux-dependent encounter frequency is larger than the activation rate and because the flux-dependent process is no longer rate limiting. The structural requisites for flux coupling require that there is a multi-ion long pore region between the binding site and the intracellular end of the ion pathway and that there must always be at least one K^+ ion present so that flux coupling can take place in the long pore [1,34]. The monotonic voltage-dependent increase in k_{off} over +10 mV to +100 mV suggests that Ba^{2+} from the intracellular side may dissociate outward to the extracellular solution over the range of the test pulses. The unbinding process does not contribute to the steep decrease in K_d at voltages within +40 mV above E_K in internal Ba^{2+} block. The increase of K_d at voltages positive to +40 mV was due to the fact that Ba^{2+} may dissociate to the external solution with a $z\delta$ for $k_{off} = 0.78$, whereas the $z\delta$ for k_{on} is only 0.11 in this voltage range. The relations between K_d and voltage (Fig. 3E) result from a combination of the flux-dependent encounter frequency of Ba^{2+} with the binding site and the simple outward dissociation process of the Ba^{2+} ion from the binding site.

3.5. Dissociation rates of the long tail in the E224G mutant are the same whether Ba^{2+} is present or absent during the recovery phase

The recovery rate of the long tail was measured in E224G. The voltage was stepped from the steady-state block at +40 mV to negative voltages (from −10 mV to −160 mV), and the apparent unbinding rate was estimated by the relation $k_{off} = 1/\tau$. As shown in Fig. 3C and F, the k_{off} values in E224G at various voltages were almost the same as those in the wild type (Fig. 2F), which indicates that the high-affinity binding site for Ba^{2+} is not affected by the E224G mutation. As we know, the relaxation rates in a one-to-one binding reaction may be affected by the binding rate as well as by the unbinding rate according to the following: the time constant $\tau = 1/(k_{on}[Ba^{2+}] + k_{off})$. To ensure that the measured recovery rates of the long tails at various voltages

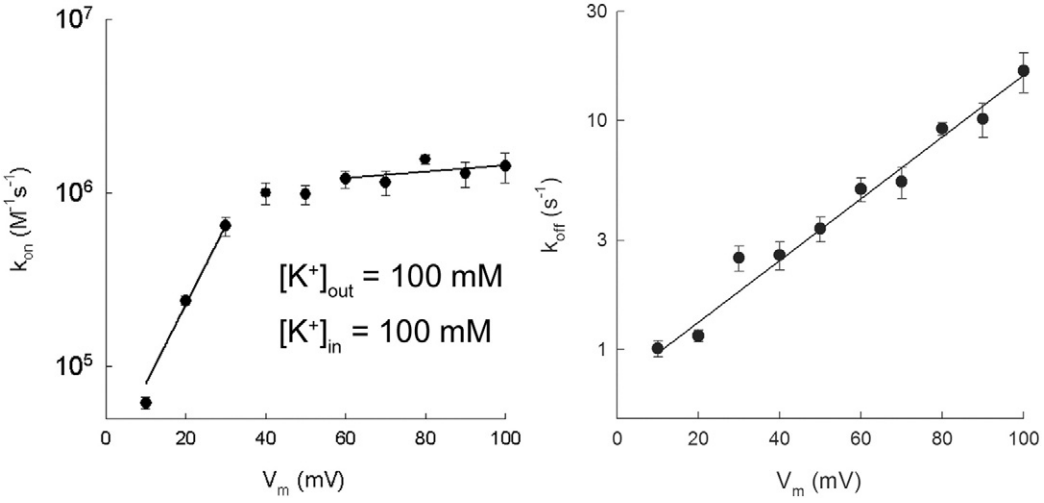

Fig. 4. k_{on} and k_{off} of the block of outward currents in the E224G mutant in 10 μM internal Ba^{2+} in $[K^+]_{out} = 100$ mM and $[K^+]_{in} = 100$ mM. k_{on} increases sharply with the voltage from +10 mV to +30 mV. The coefficients using a single exponential fit are as follows: $k_{on}(0) = 2.79 \pm 0.68 \times 10^4\ M^{-1}\ s^{-1}$ and $z\delta = 2.62 \pm 0.61$. At voltages above +40 mV, k_{on} increases, with milder voltage dependence. The coefficients of the fit from +60 mV to +100 mV are as follows: $k_{on}(0) = 9.39 \pm 0.30 \times 10^5\ M^{-1}\ s^{-1}$ and $z\delta = 0.11 \pm 0.10$. In contrast, the k_{off} values have monotonic voltage dependence from +10 mV to +100 mV. The line is the best fit: $k_{off}(0) = 0.71 \pm 0.13\ s^{-1}$ and $z\delta = 0.78 \pm 0.05$ (n = 4–10).

actually reflected the unbinding rates of the Ba^{2+} and were not affected by the binding process (i.e., the $k_{on}[Ba^{2+}]$ term), we performed two groups of experiments when measuring the recovery rate. In one group, the whole process was carried out in the presence of 10 μM internal Ba^{2+}, including the recovery process. In the other group, the internal solution was changed to the control solution without Ba^{2+} during the recovery process using the electric stepper motor (Fig. 3C). The k_{off} values in both groups were the same over −10 mV to −160 mV (Fig. 3F), which indicates that the binding process contributes little to the recovery rate; therefore, we can be confident that the recovery rate is the unbinding rate of the Ba^{2+} from the high-affinity binding site.

The implication of the results is that once the Ba^{2+} ion dissociates from the binding site, either to the extracellular or to the intracellular solution, the K^+ ions immediately flow inward and prevent the internal Ba^{2+} from binding to the site. We can infer that there must be at least one K^+ ion always present in the pathway between the high-affinity binding site and the cytoplasmic solution. This idea is supported by a structural study that revealed a K^+ binding site at the cytoplasmic domain of the Kir2.1 channel, although the K^+ ion was not fully dehydrated [25]. The low apparent affinity to Ba^{2+} of the Kir2.1 channel at voltages negative to E_K may result from the low apparent binding rate rather than from the large unbinding rate. For example, the k_{off} at −100 mV is 0.25 s^{-1}; however, even 1 mM internal Ba^{2+} can hardly bind to the high-affinity binding site. Therefore, the apparent binding rate is very small at −100 mV, when the probability of encounter between Ba^{2+} and the binding site is very low, because the inner ion binding sites along the cytoplasmic side of the narrow, long pore are nearly always occupied by K^+ ions. Furthermore, the continuous inward K^+ ion flux and the resulting flux-coupling effect prevent the cytoplasmic Ba^{2+} ions from encountering the high-affinity Ba^{2+} binding site.

3.6. Inward rectification is "driving force"-dependent, by changing either the external K^+ or the internal K^+ concentrations

A feature of the I–V_m relations of inward rectifier K^+ channels is that the steep voltage dependence near the equilibrium potential shifts with the equilibrium potential. Thus, we examined the effect of driving force on the block of the outward currents by internal Ba^{2+} in E224G. The relations between the relative currents and the test voltage were compared in four K^+ ionic conditions: $[K^+]_{out}/[K^+]_{in}$ = 100 mM/100 mM (E_K = 0 mV), 20 mM/100 mM (E_K = −40 mV), 100 mM/500 mM (E_K = −40 mV), and 500 mM/500 mM (E_K = 0 mV). Fig. 5 shows the relative currents in 10 μM internal Ba^{2+}. The extent of the block was highly correlated with the driving force ($V_m - E_K$) rather than with V_m alone. When $[K^+]_{out}/[K^+]_{in}$ = 100 mM/100 mM or 500 mM/500 mM, the steep voltage dependence of the block was observed from +10 mV to +40 mV. A smaller fraction of the channel was blocked in 500 mM/500 mM than in 100 mM/100 mM due to the competition of the Ba^{2+} with K^+ ions. When compared with the relative currents in 100 mM/100 mM, the relative currents shifted leftward to the same extent as the E_K shift (from 0 mV to −40 mV), regardless of whether we decreased the external $[K^+]$ to 20 mM or increased the internal $[K^+]$ to 500 mM. When $[K^+]_{out}/[K^+]_{in}$ = 20 mM/100 mM or 100 mM/500 mM, the extent of the block increased, with steep voltage dependence from −30 mV to + 10 mV. In all four of the ionic conditions, the block began when the voltage was above E_K, and the extent of the block reached a maximum when V_m was 40 mV to 50 mV more positive than E_K. These results reveal that internal Ba^{2+}-mediated block of the outward current is significantly affected by the driving force of K^+ flux, regardless of whether the E_K was adjusted by changing the external or internal K^+ concentration. We decided not to attribute the leftward shift of the relative current curve when $[K^+]_{out}/[K^+]_{in}$ = 20 mM/100 mM as a result of weakened competition between the external K^+ and the internal Ba^{2+} as some previous studies have suggested because in 100 mM/500 mM, the relative currents also shifted leftward. The voltage dependence of the block could not be attributed to the electrical potential alone; if the voltage dependence was due to the electrical potential alone, the block should have the same voltage dependence over the same voltage range in various K^+ ionic conditions. A plausible mechanism for the strong inward rectification is that the driving force ($V_m - E_K$), which is equivalent to the difference of the electrochemical potentials across the membrane, determined the direction and magnitude of the K^+ ion flux. The movement of the Ba^{2+} ion is significantly coupled to the K^+ flux along the narrow and long cytoplasmic pore of the Kir channels, and thus the blocking action is highly dependent on the driving force.

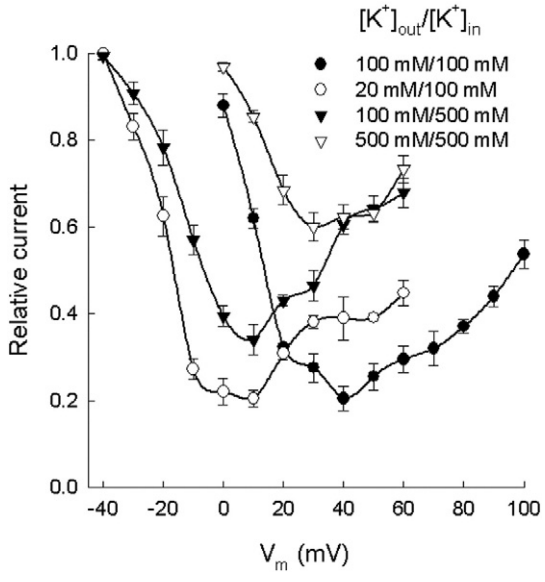

Fig. 5. Effect of driving force on the block of the outward currents in E224G in 10 μM internal Ba^{2+}. The extent of block shifts with the driving force of K^+ ion flux. E_K is −40 mV when $[K^+]_{out}/[K^+]_{in}$ = 20 mM/100 mM or 100 mM/500 mM. In all of the K^+ ionic conditions shown here, the block takes place when the voltage is positive to E_K, and the extent of block is greatest when $V_m - E_K$ = 40 mV to 50 mV. The relative currents at E_K were measured from the ratio of the initial recovery (the beginning of the long tail) to the steady current at −100 mV (n = 4–8).

Kinetic analysis of the block by internal Ba^{2+} was performed in the various ionic conditions described above. As shown in Fig. 6, in the conditions $[K^+]_{out}/[K^+]_{in}$ = 20 mM/100 mM or 100 mM/500 mM, when E_K = −40 mV in both groups, the k_{on} values increased steeply from −30 mV to +10 mV and reached more steady values at voltages above +20 mV. In 500 mM/500 mM $[K^+]$, the steep increase of k_{on} took place at voltages from +10 mV to +40 mV. The k_{off} values in all groups showed monotonic voltage dependence over the test voltages. The kinetic results in 100 mM/100 mM $[K^+]$ are shown in Fig. 4. The fit results using single exponentials in Fig. 6 are as follows: (A) $[K^+]_{out}/[K^+]_{in}$ = 20 mM/100 mM: at −30 mV to −10 mV, $k_{on}(0) = 1.58 \pm 0.00 \times 10^6$ M^{-1} s^{-1} and $z\delta = 3.24 \pm 0.01$; at +20 mV to +60 mV, $k_{on}(0) = 1.52 \pm 0.27 \times 10^6$ M^{-1} s^{-1} and $z\delta = 0.27 \pm 0.01$; $k_{off}(0) = 4.50 \pm 0.72$ s^{-1} and $z\delta = 0.69 \pm 0.08$. (B) $[K^+]_{out}/[K^+]_{in}$ = 100 mM/500 mM: at −30 mV to −10 mV, $k_{on}(0) = 5.48 \pm 0.65 \times 10^5$ M^{-1} s^{-1} and $z\delta = 3.14 \pm 0.27$; at +20 mV to +50 mV, $k_{on}(0) = 7.15 \pm 1.26 \times 10^5$ M^{-1} s^{-1} and $z\delta = 0.27 \pm 0.11$; $k_{off}(0) = 3.08 \pm 0.50$ s^{-1} and $z\delta = 0.99 \pm 0.09$. (C) $[K^+]_{out}/[K^+]_{in}$ = 500 mM/500 mM: at +10 mV to +30 mV, $k_{on}(0) = 1.76 \pm 1.03 \times 10^4$ M^{-1} s^{-1} and $z\delta = 2.22 \pm 0.51$; $k_{off}(0) = 1.58 \pm 0.57$ s^{-1} and $z\delta = 0.95 \pm 0.17$. In the four ionic conditions, the steep voltage dependence of the block from E_K to E_K + 40 mV was caused by the steep increase of k_{on}, which results from the sharp increase in the encounter frequency determined by the flux-coupling effects.

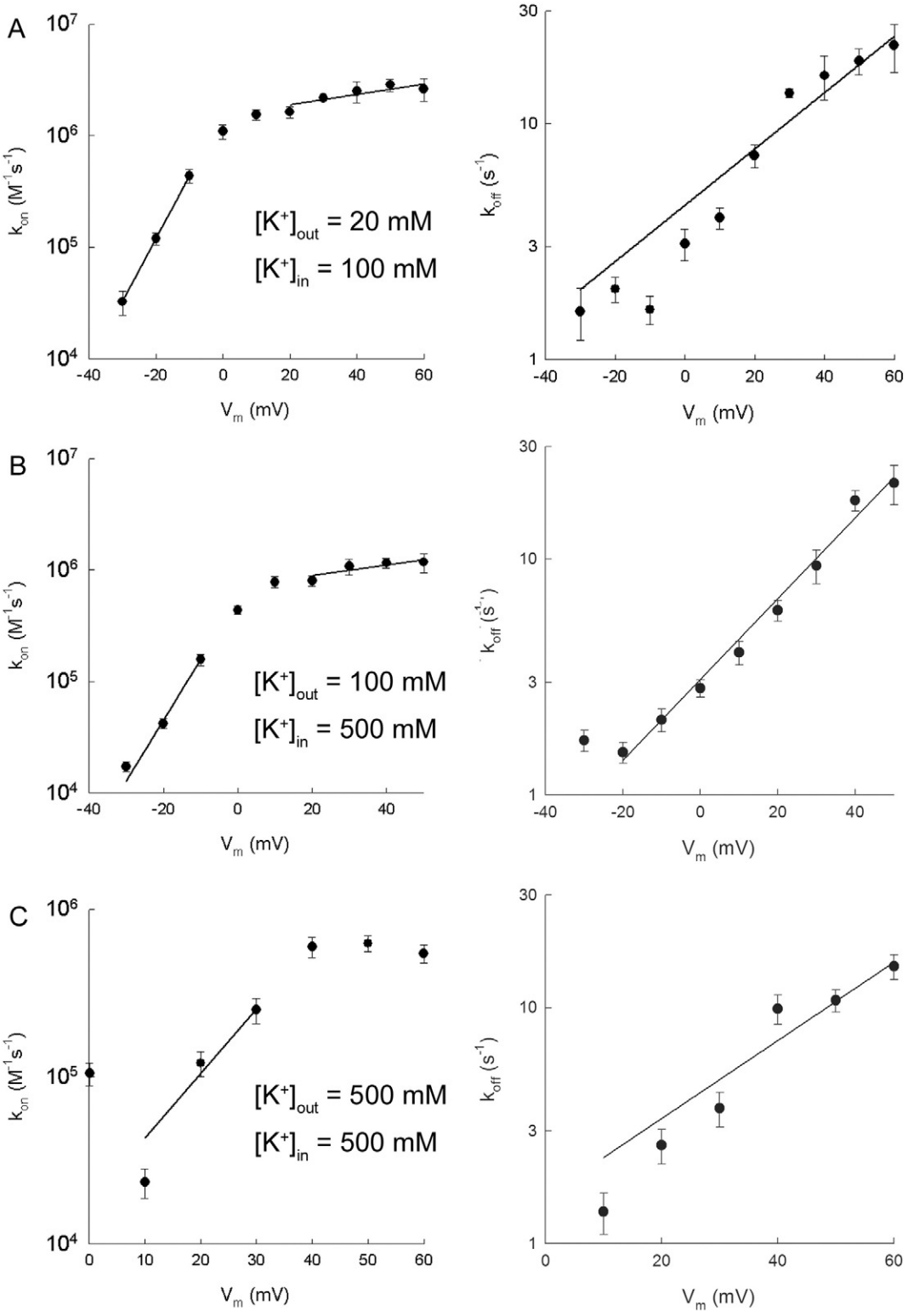

Fig. 6. k_{on} and k_{off} of the block of E224G outward currents in 10 μM internal Ba^{2+} in various K^+ concentrations. $[K^+]_{out}/[K^+]_{in}$ = 20/100, 100/500, and 500/500 mM in (A), (B), and (C), respectively (n = 4–7).

3.7. Flux-dependent block of the inward K^+ current could occur at voltages near but negative to E_K

From the results and discussion above, we know that the inward rectification in internal Ba^{2+} block is caused by the flux-dependent block. When the K^+ flux is outward, the blocker is coupled with the flow and reaches the binding site. When the K^+ flux is inward, the blocker has little access to the binding site because the inwardly flowing K^+ ions prevent the blocker from encountering the binding site. However, the block at voltages near E_K requires special consideration. In symmetric K^+ concentrations, when E_K is 0 mV, the inward currents at negative voltages near E_K can be blocked by higher concentrations of internal blockers. The block of inward currents by spermine at voltages negative to E_K has been studied in single-channel recordings [38]. When the

internal [Ba^{2+}] was raised to 1 mM or 3 mM in 100 mM/100 mM [K^+], the inward currents at voltages of −20 mV or −10 mV were partially blocked, and the recovery phase had a long tail as well (not shown), which suggests that the Ba^{2+} interacted with the same high-affinity site described above. In our interpretation of the flux-dependent block, the blocking action is coupled with the K^+ flux. One might then ask why there is a block of inward currents at voltages near E_K. As we know, the net K^+ flux is the difference between the efflux and influx. At the equilibrium potential, the efflux equals the influx, and the net flux is zero. At voltages near and negative to E_K, the net flux is inward; however, there is still some unidirectional outward flux. The ratio of the unidirectional efflux and the influx has been described with radioactive tracers using the Ussing flux ratio equation [39,40]:

$$\frac{J_{outward}}{J_{inward}} = \frac{[K^+]_i}{[K^+]_o}\exp\left(\frac{zFV_m}{RT}\right) = \exp\left(\frac{z(V_m - E_K)F}{RT}\right). \quad (6)$$

Hence, when the concentration of the internal blocker is higher, it is possible for the blocker to reach the binding sites because the blocker could be coupled with the unidirectional K^+ efflux. Higher concentrations of positively charged blockers have another effect on the inward current; they reduce the current amplitude by shielding the negative charges at the inner vestibules of the channels [38].

Another strategy of observing the block of the inward currents near E_K is to reduce the intracellular K^+ concentration. When the intracellular K^+ concentration is lowered, the competition effect is weakened and the cytoplasmic pore is less saturated by the K^+ ions; therefore, the internal Ba^{2+} could have greater access to enter to the pore and to bind with the high-affinity site. Here, we examined the effects of internal Ba^{2+} on currents in the E224G mutant in $[K^+]_{out}/[K^+]_{in}$ = 20 mM/20 mM. Ba^{2+}-mediated block of the inward currents near E_K becomes obvious in this ionic condition. K_d values at various voltages were estimated using Eq. (1). Fig. 7A shows the dose dependence of the block in 0.3 μM, 1 μM, 3 μM, and 10 μM internal Ba^{2+}. Approximately 20% of the inward current at −20 mV was blocked, and approximately 50% was blocked at −10 mV by 10 μM internal Ba^{2+} (Fig. 7C and D). The relative currents at E_K can be estimated by measuring the ratio at the initial recovery when the voltage was stepped back to −100 mV. The K_d values steeply decreased from −20 mV to +10 mV and reached more steady values at voltages above + 20 mV. At −20 mV to +10 mV, the fits using a single exponential were as follows: $K_d(0) = 2.18 \pm 0.17$ μM and $z\delta = 3.21 \pm 0.08$. The kinetic analysis of the blocking showed that k_{on} values increased steeply with voltage from −10 mV to +20 mV and reached more steady values at voltages above +30 mV (Fig. 7E). The k_{off} values had a monotonic voltage dependence from −10 mV to +70 mV, with $z\delta = 0.82 \pm 0.10$. The binding of the Ba^{2+} ions to the high-affinity site was the same at −20 mV or −10 mV as they were at positive voltages. The block by internal Ba^{2+} at voltages near and negative to E_K reflects the fact that there is a significant probability of outward unidirectional flux, although the net flux is inward at these voltages. Thus, the mechanism we proposed for the flux-dependent block is appropriate, even when interpreting the block at voltages near and negative to E_K.

3.8. A "driving force"-dependent block can be demonstrated in various external [K^+] at 0 mV, when there is no transmembrane electrical field

We have shown that the inward rectification of Kir2.1 channels may be due to the flux-coupling effect. The direction and magnitude of the K^+ flux significantly affect the apparent binding rate of internal Ba^{2+}. The block mediated by the internal Ba^{2+} depends on the driving force ($V_m - E_K$), rather than on V_m alone. The large $z\delta$ values (~3) of K_d near E_K may arise from the flux-dependent encounter frequency and thus from the flux-dependent k_{on}. However, the conventional interpretation of the $z\delta$ near E_K is that the steep voltage dependence is due to the fact that several K^+ ions have to move concertedly across the electrical field to allow the blocker to bind to the binding site [1,2,6,34]. The difference between the conventional interpretation and our flux-coupling interpretation of the steep voltage dependence of the block near E_K is subtle and interesting. Here, we wish to introduce an experiment to emphasize the idea of the flux-dependent block. We will show that the block is steeply dependent on the driving force even when the K^+ flux is driven by diffusion alone, a condition in which there is no voltage difference across the membrane. Before doing so, it is useful to review the concepts of the driving force.

As we know, the driving force for K^+ ion flux across membrane channels is the difference of the electrochemical potentials across the membrane.

$$\tilde{\mu} = \mu^o + RT\ln c + zFV, \quad (7)$$

where c is the concentration, z is the valence of the ion, and F, R, and T have their usual thermodynamic meanings. The ion flux across a membrane can be empirically expressed as [41]:

$$J = L\Delta\tilde{\mu}, \quad (8)$$

where J is the flux due to electrodiffusion, L is a proportional constant, and $\Delta\tilde{\mu}$ is the difference of the electrochemical potentials across the membrane, $(\tilde{\mu}_{in} - \tilde{\mu}_{out})$.

$$\begin{aligned}\Delta\tilde{\mu} &= \tilde{\mu}_{in} - \tilde{\mu}_{out} = RT\ln\frac{c_{in}}{c_{out}} + zF(V_{in} - V_{out})\\ &= zF\left(\frac{RT}{zF}\ln\frac{c_{in}}{c_{out}} + (V_{in} - V_{out})\right),\end{aligned} \quad (9)$$

or, equivalently,

$$\Delta\tilde{\mu} = zF(V_m - E_K). \quad (10)$$

Eq. (8) has the same meaning as the empirical formula $I = G(V_m - E_K)$ commonly used by electrophysiologists. Therefore, the driving force ($V_m - E_K$) is equivalent to the difference of the electrochemical potentials across the membrane.

Let us consider a condition in which there is no voltage difference (V_m = 0 mV) across the membrane. The flux is due to diffusion, not electrodiffusion, and there is no electrical field across the membrane channel in this case. The driving force is the difference of the chemical potentials across the membrane. The chemical potential is defined as:

$$\mu = \mu^o + RT\ln c. \quad (11)$$

The flux can be expressed as:

$$J = L\Delta\mu, \quad (12)$$

where $\Delta\mu$ is the difference of the chemical potentials across the membrane, $(\mu_{in} - \mu_{out})$.

$$\Delta\mu = \mu_{in} - \mu_{out} = RT\ln\frac{c_{in}}{c_{out}}, \quad (13)$$

or,

$$\Delta\mu = zF(-E_K). \quad (14)$$

Hence, the driving force for the ion flux at 0 mV is the difference of the chemical potentials across the membrane, which is proportional to $(-E_K)$ and to the flux

$$J = L\Delta\mu \propto (-E_K). \quad (15)$$

To study the flux-dependent block by internal Ba^{2+} when the K^+ flux is due to diffusion but not electrodiffusion, we changed the external K^+ concentration in different patches, while keeping the internal K^+

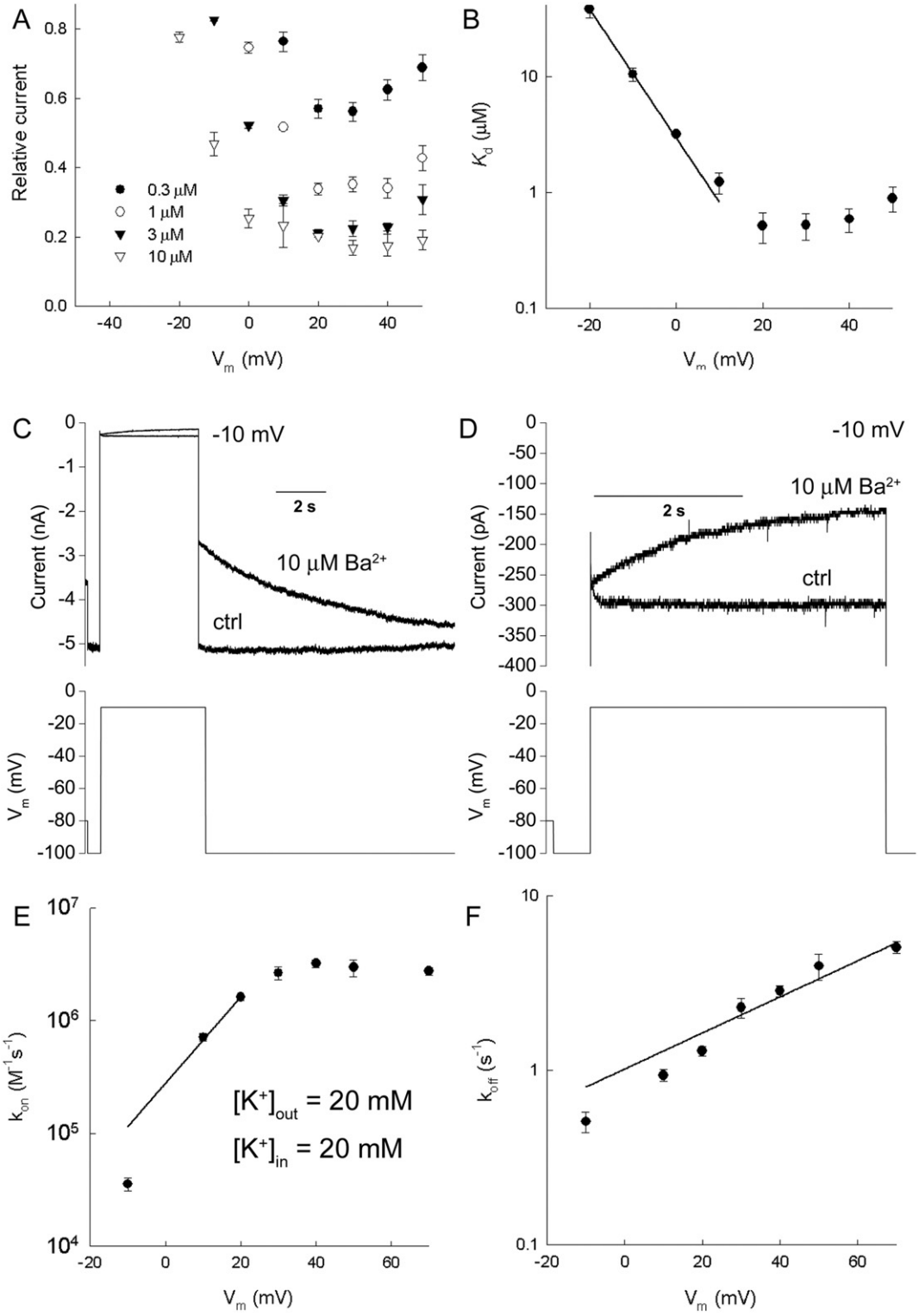

Fig. 7. Block of the E224G currents by internal Ba^{2+} when extracellular and intracellular $[K^+]$ are both 20 mM. (A) Dose dependence and voltage dependence of the block. Note that the inward currents at −20 mV and −10 mV are significantly blocked by 10 μM Ba^{2+}, even though an E_K of 0 mV is the experimental condition. The relative currents at 0 mV were measured from the ratio of the initial recovery (the beginning of the long tail) to the steady current at −100 mV (B) K_d is plotted against the voltage. K_d decreases steeply ($z\delta = -3.21 \pm 0.08$) at voltages from −20 mV to +10 mV and then increases mildly from +20 mV to +50 mV ($n = 3$–5). (C) At the test voltage of −10 mV, 10 μM internal Ba^{2+} blocked ~50% of the inward current. (D) Enlarged view of the inward currents at −10 mV in Ba^{2+} and in control conditions. (E) k_{on} is estimated from the data obtained during the block by 3 μM internal Ba^{2+}. k_{on} increases steeply from −10 mV to +30 mV and then reaches a steady value. (F) k_{off} shows monotonic voltage dependence, with $z\delta = 0.82 \pm 0.10$. $k_{off}(0) = 2.23 \pm 0.39\ M^{-1}\ s^{-1}$.

concentration at 100 mM. The voltage of the test pulses was 0 mV, so there was no electrical field across the membrane channel. Then, we plotted the relative currents recorded in 10 μM internal Ba^{2+} against $\Delta\mu$ (Fig. 8A). For example, when the external $[K^+]$ was 37 mM, the $\Delta\mu$ was 1 RT; when the external $[K^+]$ was 20 mM, the $\Delta\mu$ was 1.61 RT. The results show that the block by internal Ba^{2+} was dependent on $\Delta\mu$. When $\Delta\mu < 0$, the K^+ flux was inward, and there was little block. When $\Delta\mu > 0$, the K^+ flux was outward, and the extent of the block

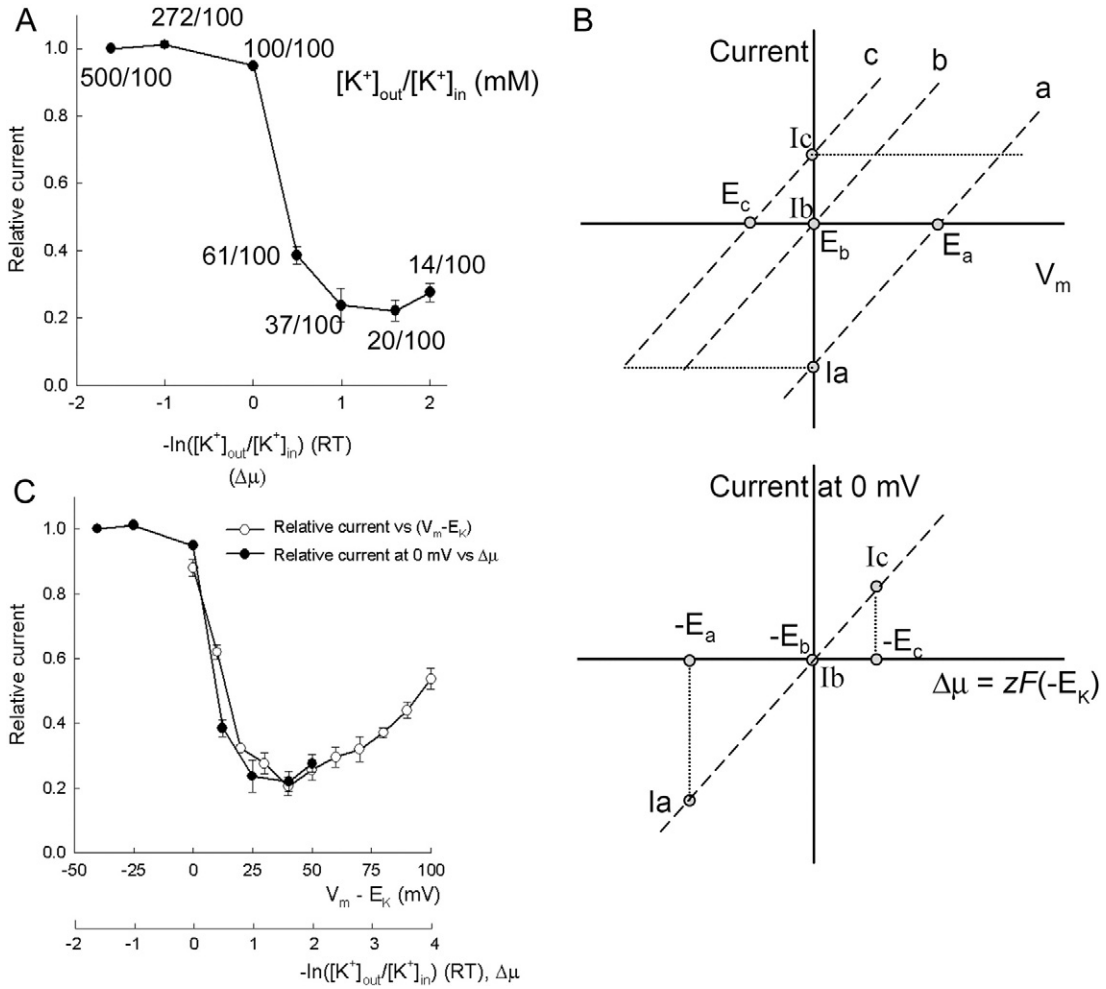

Fig. 8. (A) Block of E224G outward currents by 10 μM internal Ba^{2+} with different driving forces at 0 mV. The relative currents were plotted against the driving force at 0 mV or against the chemical potential difference ($\Delta\mu$) across the membrane. Different driving forces were obtained by changing the external K^+ concentration of the pipette solution in inside-out recordings while maintaining the internal K^+ concentration at 100 mM for all of the experiments presented here. The extent of the block by internal Ba^{2+} depends on the direction and magnitude of the driving force for K^+ ion flux. The results suggest that the block by internal Ba^{2+} strongly depends on the direction of the K^+ flux, even when there is no voltage difference across the membrane (Vm = 0 mV). The relative currents at E_K were measured from the ratio of the initial recovery currents when the voltage was stepped back to −100 mV (n = 4–7). (B) Interpretation of the driving force at 0 mV. When the equilibrium potential is E_c and $E_c < 0$ mV, the current at 0 mV, Ic, is outward. When the equilibrium potential is E_a and $E_a > 0$ mV, the current at 0 mV, Ia, is inward. If we plot the curves of the current at 0 mV against $(-E_K)$, we obtain the curve in the lower panel. Note that $(-E_K)$ is proportional to the chemical potential difference $\Delta\mu$. (C) Comparison of the curve in (A) and the relative current vs. $(V_m - E_K)$ at $[K^+]_{out}/[K^+]_{in}$ = 100 mM/100 mM.

increased steeply with $\Delta\mu$ from 0 to 1.6 RT. As shown in Fig. 8C, when the curve of the relative current vs. $\Delta\mu$ obtained using this method is compared with the curve of the relative current vs. V_m obtained in the previous experiment, when $[K^+]_{out}/[K^+]_{in}$ = 100 mM/100 mM (from Fig. 3D, 10 μM Ba^{2+}), the two curves can nearly be superimposed. Although the horizontal axes of the two experiments seem to have different physical units, they both mean the "driving force" for electrodiffusion or for diffusion, or more generally, the electrochemical potential gradient across the membrane. Therefore, we can conclude that the block by internal Ba^{2+} is flux-dependent or driving force-dependent, regardless of whether the K^+ flux is driven by the electrical potential gradient or concentration gradient alone. The comparison in Fig. 8C suggests that the steep driving force-dependence of the extent of the block near the equilibrium position ($\Delta\tilde{\mu} = 0$) may not result from the electrical potential drop caused by the blocker and the migrating K^+ ions when they cross the electrical field. As shown in Fig. 8A, when the driving force for the K^+ flux was equal to the concentration difference, but not to the electrical potential difference, the extent of the block steeply increased when $\Delta\mu$ increased from 0 to 1.6 RT. As we know, the electrical potential difference at 25 mV is approximately 1 RT. A chemical potential difference of 1.6 RT produced a block similar to the block observed at +40 mV in 100 mM/100 mM $[K^+]$, the condition in which the block was maximal in both experiments (Fig. 8C). One may question whether the K^+ flux and the Ba^{2+}-mediated block by are also affected by the K^+ concentrations. In our experiments here, the internal K^+ concentration was always 100 mM, so the competition effect due to the internal K^+ should not differ between the experiments.

3.9. A mutagenesis study reveals that the high-affinity binding site for internal Ba^{2+} is near T141

In our studies of internal Ba^{2+} block of outward currents, we have shown that the recovery rates are slow when the voltages are stepped back to negative voltages in both the wild-type (Fig. 2C) and in the E224G channels (Fig. 3C). The slow unbinding rate may reflect a high activation barrier for dissociation from the high-affinity binding site. The unbinding rate of Ba^{2+} mainly depends on the intrinsic chemical affinity of Ba^{2+} with the coordinating ligands at the binding site and depends less on the K^+ flux. With this in mind, we tried to identify the location of the high-affinity binding site for the internal Ba^{2+} by mutating the residues and checking the effect of the mutation on the recovery rate. Based on the literature, several mutants that might affect ion binding

in the pore were constructed. In addition to E224G, we constructed D172N [15,42–45], D172N–E224G [15], C169V [46], S165L [21,47–49], T141A [16,17,21,48], and T141A–S165L [48]. A Rasmol model of the structure of the Kir2.1 channel is shown in Fig. 9C; the corresponding locations of the mutated residues were labeled. The model retrieved from the SWISS-MODEL Repository [50] is based on the X-ray crystallography template structure of a Kir2.2 channel (PDB: 3sph) [22].

The recovery rates when the voltage was stepped back to −100 mV from the steady-state Ba^{2+} block of the outward currents are compared in Fig. 9A and B. Markedly, the T141A mutant had a 25-fold faster recovery rate ($\tau = 163$ ms, $k_{off} = 6.33\ s^{-1}$ at −100 mV) than the wild-type ($\tau = 4$ s, $k_{off} = 0.25\ s^{-1}$ at −100 mV). The double mutant T141A–S165L almost abolished the high-affinity Ba^{2+} binding site, and the current was not affected by even 1 mM internal Ba^{2+}. The several other mutants tested, including D172N, E224G, D172N–E224G, C169V, and S165L, had similar recovery rates as the wild-type channel.

We then examined the recovery rates in T141A at various voltages from −10 mV to −160 mV. The k_{off} values increased when the voltage became more negative, with a voltage dependence ($z\delta = -0.17 \pm 0.01$) from −10 mV to −160 mV. In contrast with the recovery rates of the long tails in the wild type, the k_{off} values in T141A showed monotonic voltage dependence over the range of test voltages. The activation barrier for Ba^{2+} to dissociate inwards from the binding site seems to be reduced in the T141A mutant, and the Ba^{2+} preferentially dissociated to the cytoplasmic solution at voltages from −10 mV to −160 mV. The high-affinity binding site for internal Ba^{2+} is probably located near T141, which is the residue just before the TIGYG (residues 142 to 146) signature sequence of the selectivity filter. T141 is located at the conjunction of the pore helix and the selectivity filter and is the internal entrance of the selectivity filter. A mutation near the T141 site has been shown to lower the binding affinity when Ba^{2+} was applied from the external solution to block the inward K^+ currents [16,17,21]. Our result

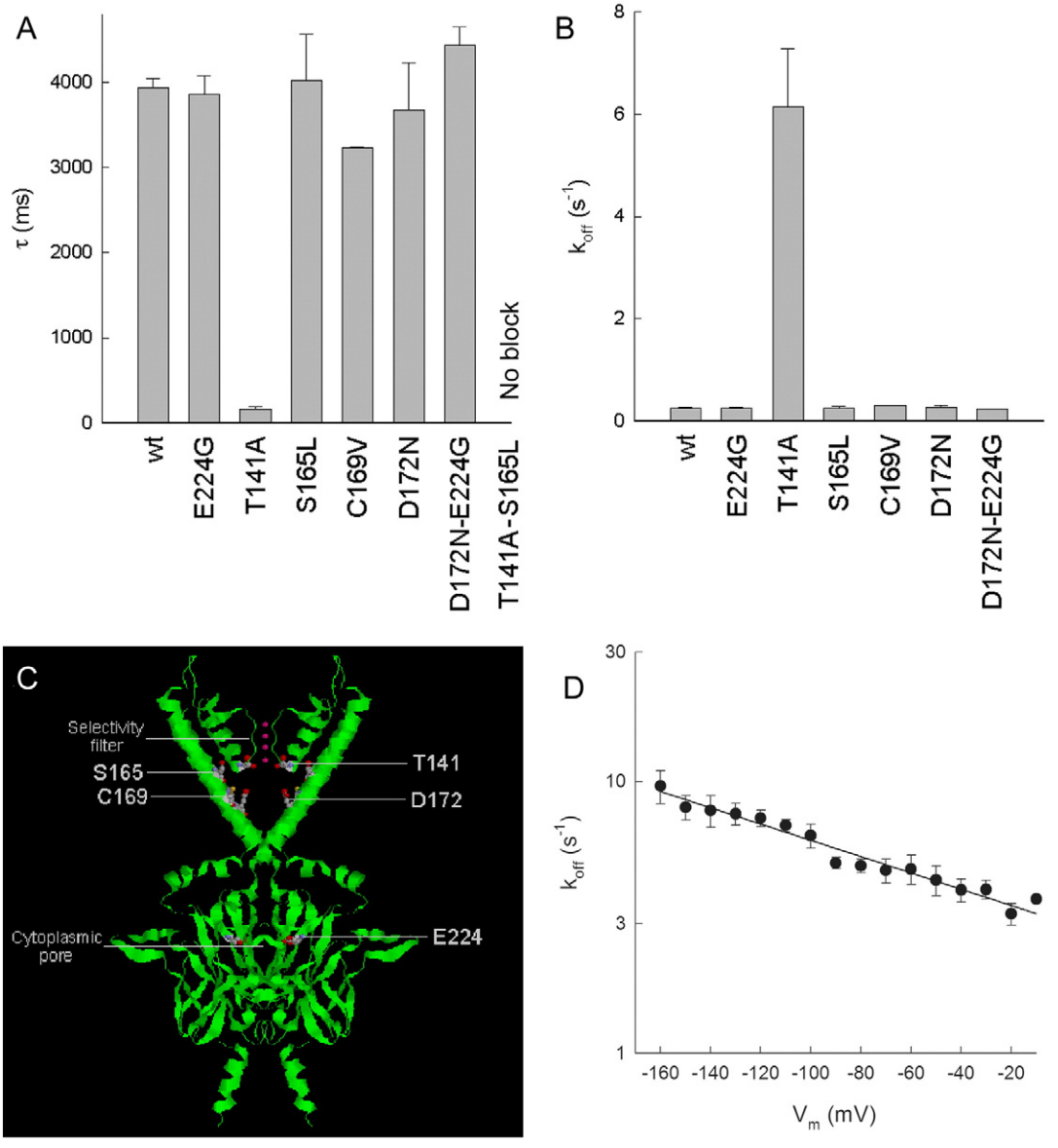

Fig. 9. Mutagenesis studies to compare the dissociation kinetics in the wild-type and mutant Kir2.1 channels. (A, B) The kinetics of the recovery at −100 mV from the internal Ba^{2+} (10 μM) block in the wild-type or mutants are shown. The currents were elicited to +40 mV or +60 mV and were stepped back to −100 mV. In E224G, S165L, C169V, D172N, and D172N–E224G, the τ of the recovery is 3 s to 4 s, similar to the rate in the wild-type. In T141A, the recovery is 25 times faster than in the wild-type. The τ is 163 ± 30 ms ($k_{off} = 6.33 \pm 0.65\ s^{-1}$). The results suggest that the high-affinity binding site may be near T141 ($n = 4$–8). The double mutant T141A–S165L was not affected by 1 mM Ba^{2+}. (C) Model of the structure based on the X-ray crystallography template structure of a Kir2.2 channel (PDB: 3sph) [22] of the Kir2.1 channel is shown with Rasmol. Only two chains are shown here. The residues we have mutated in this study are shown in "ball and stick" mode. (D) The k_{off} of T141A shows monotonic voltage dependence from −160 mV to −10 mV, with $k_{off}(0) = 3.05 \pm 0.13\ s^{-1}$ and $z\delta = -0.17 \pm 0.01$.

may be the first study demonstrating that T141 is a key site of Ba^{2+} block when the Ba^{2+} is applied from the cytoplasmic side to block the outward K^+ currents. This Ba^{2+} binding site corresponds well with the Ba^{2+} binding site in the KcsA channel revealed by X-ray crystallography [51]. Our mutagenesis studies show that the cytoplasmic Ba^{2+} ion has to traverse the narrow cytoplasmic pore to reach the high-affinity binding site near the site of T141, which is just adjacent to the internal end of the selectivity filter. The cytoplasmic pore is a narrow and long structure with K^+ ion binding sites. Several structural studies have revealed that the single-file region in Kir channels may extend from the selectivity filter to the cytoplasmic domain [23,25,52]; in contract, most other K^+ channels have a single-file region only along the selectivity filter. The unique structural elements of the single-file, multi-ion long cytoplasmic pore in Kir channels facilitates the flux-coupling effect by conducting K^+ ions with the blocking ion and contributes to the driving force-dependent block and the resulting inward rectification phenomenon.

4. Discussion

4.1. Flux-dependent block accounts for the inward rectification in Ba^{2+}-mediated blockage of the Kir2.1 channel

We provide evidence that the inward rectification of the blocking action by internal Ba^{2+} ions in Kir2.1 channels is mainly due to the flux-coupling effect. The movement of the Ba^{2+} ions is strongly coupled with the K^+ ion flux in the narrow and long cytoplasmic pore, and thus the encounter frequency of the Ba^{2+} with the high-affinity binding site is significantly influenced by the direction and the magnitude of the K^+ flux. The steep decrease in the apparent dissociation constant near E_K results from the steep increase in the apparent binding rate constant, which is determined by the encounter frequency. In Ba^{2+} block, the rate of unbinding from the binding site is chiefly determined by the energy profile of the binding site. The idea that the flux of the permeating ions may influence the apparent affinity of the pore blocker has been proposed for Ca^{2+} channels and Na^+ channels [53–55].

The driving force for K^+ flux through membrane channels is the electrochemical potential difference across the membrane, that is, $(V_m - E_K)$, or $\Delta\tilde{\mu}$. When the electrochemical potential of the extracellular solution is larger than that of the intracellular solution, the K^+ flux is inward; when the intracellular solution has a larger electrochemical potential, the K^+ flux is outward. For strong inward rectification to occur, the blocking action has to be highly coupled with the driving force, such that only the outward flux is occluded while the inward flux is unaffected by the blocker. The inward rectifier channels are equipped with the cytoplasmic pore, a multi-ion long pore that facilitates the directional diffusion or electrodiffusion and the flux-coupling effect.

We demonstrate that the flux-dependent block takes place even when the K^+ flux is driven by the concentration difference alone, when there is no electrical potential difference across the membrane (Fig. 8). In this case, the driving force is the chemical potential difference but not the electrochemical potential difference, and the flux is due to diffusion rather than electrodiffusion. As shown in Fig. 8C, the extent of the block is dependent on the driving force regardless of whether the driving force results from a chemical potential difference or from an electrical potential difference. The results are significant in that the steep voltage dependence near E_K in the I–V_m curve of Kir channels may be not caused by the electrical potential drop due to the charge of the blocker or of the K^+ ions across the electrical field. It appears to be unsatisfactory to attribute the steep voltage dependence and the large $z\delta$ near E_K to the fact that several K^+ ions have to move across part of the electrical field to allow the blocker to bind to the binding site [1,2,6,34]. Our study shows that the inward rectification of internal Ba^{2+} block in Kir2.1 channels results from the "driving force"-dependent or flux-dependent block, when the K^+ flux is driven by the concentration gradient alone or by the electrochemical potential gradient of K^+ ions across the membrane.

4.2. The single-file, multi-ion cytoplasmic pore of the Kir2.1 channel is a key structural determinant of the flux-coupling effect

The flux-coupling effect can occur in a single-file, multi-ion long pore; in the narrow long pore, the ions cannot pass over each other and have to move concertedly in a line. Flux coupling cannot take place in a single-ion pore, where the permeating ions and the blocking ion compete for the site and where there is no directional force acting on the blocking ion. In a homogeneous bulk solution, the flux-coupling effect does not occur. As we know, macroscopically, diffusion is a phenomenon in which ions move spontaneously from regions of higher concentration to regions of lower concentration. Microscopically, diffusion is the result of the random thermal movement of each ion. In a homogeneous ionic solution, each ion is randomly pushed by the surrounding water molecules and just jiggles, without a specific direction. The correlation time between two collisions for a K^+ ion is mD/k_BT (m: mass, D: diffusion coefficient), that is, the mean time for a K^+ ion to 'forget' its initial velocity. In physiological conditions, the correlation time for the diffusion of a K^+ ion is ~10^{-13} s, during which time the ion moves less than 0.5 Å [1]. For comparison, the average distance between two K^+ ions is 25 Å in a 100 mM K^+ solution and is 43 Å in a 20 mM K^+ solution. Therefore, K^+ ions move independently of each other in a homogeneous solution; although there is a macroscopic flux due to the concentration difference, there is no flux coupling.

The single-file, multi-ion cytoplasmic pore of the Kir channels provides an anisotropic environment for the electrodiffusion or diffusion of K^+ ions. For the flux-dependent block to occur, there must be at least one K^+ ion located in the pore internal to the blocker binding site. X-ray structural studies of the cytoplasmic pore of Kir2.1 and Kir3.1 channels have revealed that the cytoplasmic pore is a narrow and long structure, which extends the K^+ ion pathway to 60 Å [23–25,52,56]. The negatively charged environment within the cytoplasmic pore may attract K^+ ions. Moreover, one or two water-caged K^+ ions were found to be present at the G-loop of the binding site in the cytoplasmic pore of the Kir2.1 and Kir 3.1 channels; thus, the single-file region may extend more than 30 Å beyond the selectivity filter [23,25]. Thus, the narrow and long cytoplasmic pore is an essential structural determinant for the inward rectification in Kir channels.

4.3. The Ussing flux ratio equation can be used to estimate the encounter frequency with the binding site near the equilibrium potential

As we have discussed, the steep increase in the apparent binding rate constant results from the flux-dependent encounter frequency of the internal Ba^{2+} with the binding site. The high-affinity binding site for the internal Ba^{2+} is near the T141 residue. Because the Ba^{2+} ion is coupled with the K^+ flux, the encounter frequency may be limited by the direction and magnitude of the K^+ flux. The blocking action of Ba^{2+} may involve several steps. First, the Ba^{2+} ions compete with the K^+ ions at the entrance of the cytoplasmic pore. Second, the Ba^{2+} ion is coupled with the outward K^+ flux and encounters the binding site. Third, the Ba^{2+} ion overcomes the activation barrier for the binding reaction and binds to the site. Then, the Ba^{2+} may dissociate to the extracellular or intracellular solution after residency at the binding site. The flux coupling in the second step is the key process that determines the steep changes of the apparent binding rate near E_K in the present study.

The detailed kinetic model of Ba^{2+} block may be complex. However, we can make a rough estimate of the encounter frequency in a hypothetical condition. Suppose that the intracellular solution contains 10 μM tracer-labeled K^+ ions and that the tracer ions have the same chemical properties as other K^+ ions; the encounter frequency of the

tracer ions to the binding site deep in the single-file pore can be estimated from the outward unidirectional flux (efflux). The efflux can be calculated from the following relations:

$$\text{Net flux} = \text{efflux} - \text{influx} \tag{16}$$

and

$$\frac{\text{Efflux}}{\text{Influx}} = \exp\left(\frac{zF(V_m - E_K)}{RT}\right)^{n'}. \tag{17}$$

Eq. (17) is the Ussing flux ratio equation raised to the n'th power [1,39,40], which gives the ratio between the efflux and the influx near the equilibrium potential. The flux-ratio exponent n' is a result of the flux coupling in a single-file, multi-ion pore nature. For example, if the ratio of the probability that a K^+ ion will be transported outwards to the probability it will be transported inwards is 1:4, the probability for a K^+ ion to be transported outwards for three consecutive steps would be 1:64. Hence, n' may indicate the number of ions in the pore needed to be transported outwards before the tracer ion encounters the binding site from the entrance of the cytoplasmic pore. The data of the net flux can be obtained from the single-channel recordings under similar recording conditions (conductance: 48 pS in the wild-type, 38 pS in E224G, at −80 mV to −140 mV in 100 mM/100 mM $[K^+]$) [13] and from the macroscopic currents at various voltages in the I–V curves. The upper limit of the apparent k_{on} of the tracer would be limited by the efflux. Fig. 10A shows the estimated efflux values in 100 mM/100 mM $[K^+]$ in E224G when $n' = 1$, 3, or 5. One can see that the efflux is sensitive to n' from negative voltages to about + 40 mV; the larger the n', the steeper the efflux increase with voltage. At voltages positive to +40 mV, the efflux is close to the outward net flux, as the probability of the outward transport approaches one. The k_{on} values of internal Ba^{2+} block increase steeply from +10 mV to +40 mV; over this voltage range, the efflux increases steeply also. At voltages positive to +40 mV, the flux-coupling effect on the apparent binding rate seems to be saturated. The apparent binding rate can be limited by the flux-dependent encounter frequency or by the activation barrier of the Ba^{2+} binding reaction. At voltages from E_K to E_K + 40 mV, the flux-dependent encounter frequency is rate limiting because it is slower than the activation rate of Ba^{2+} binding. When V_m is above E_K + 40 mV and the flux-dependent encounter frequency is larger than the intrinsic activation rate of Ba^{2+} binding, the apparent binding rate is no longer limited by the flux-dependent process, and the k_{on} values from +50 mV to +100 mV may reflect the intrinsic binding rate of the Ba^{2+} binding reaction. From these estimates, at voltages positive to +40 mV, the estimated binding rate constants of the tracer ion are approximately 60- to 80-fold larger than the k_{on} values of the internal Ba^{2+} block.

4.4. The rectification could be interpreted from a view based on the non-equilibrium thermodynamics of small systems

The Ussing flux ratio has been interpreted based on the fluctuation theorem [57]. The ratio of outward to inward unidirectional ion fluxes can be derived from the fluctuation theorem if we consider the ion channel and the solutions it contacts to be a small nonequilibrium system. Microscopically, the flux ratio is the probability of transporting a K^+ ion down the electrochemical gradient (entropy-producing) to the probability of transporting a K^+ ion against the electrochemical gradient (entropy-consuming). In this regard, the inward rectifier channel can be viewed as a Brownian nanoscale molecular machine.

It is interesting that at voltages negative and near E_K, unidirectional outward flux is possible even when the driving force predicts an inward net K^+ flux. As we demonstrated when $[K^+]_{out}/[K^+]_{in}$ = 20 mM/20 mM, the internal Ba^{2+} could reach the high-affinity binding site with considerable frequency and block the Kir2.1 channels at −20 mV, −10 mV, and even at the equilibrium potential, 0 mV (Fig. 7). The current–voltage curve never bends sharply at the equilibrium potential; instead, it rectifies smoothly, with a small "threshold" at the negative voltages near the reversal potential due to the thermodynamic limits (Fig. 11B). From a perspective based on nonequilibrium thermodynamics in small systems, the inward rectification of the Kir channels is reminiscent of the rectification in Smoluchowski's trapdoor, in the p–n diode, and in Feynman's Brownian ratchet [58,59]; backward transport can occur near the equilibrium condition, although the direction of the net transport still follows the thermodynamic driving force. In cells, the thermodynamic driving force is the concentration difference (for diffusion) or the electrochemical potential difference (for electrodiffusion) across the membrane channels. In Feynman's ratchet, it is the temperature difference of the two chambers (for heat transfer), and for the p–n diode, it is the voltage difference (for electron transport) across the p–n diode. The reversal point is determined by the driving forces and cannot be altered by the internal properties of the machine. However, if the transport barrier can be coupled to the direction of the driving force, rectification becomes possible. The strong inward rectification in Kir channels occurs because the barrier of the K^+ conduction, which is the probability of

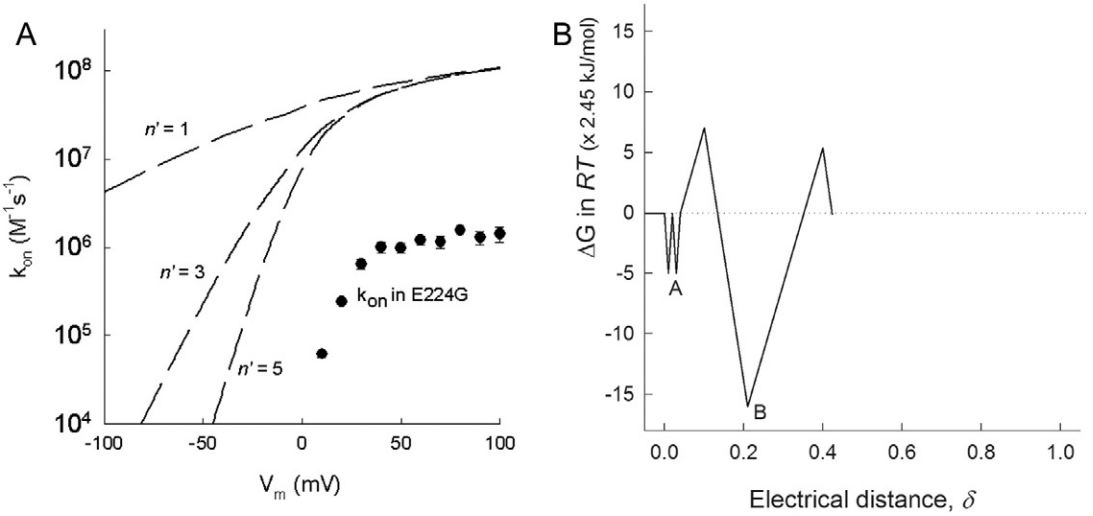

Fig. 10. (A) The estimated encounter frequency of the tracer ions obtained by calculating the unidirectional efflux when $n' = 1$, 3, or 5 in the E224G mutant. The k_{on} values of the internal Ba^{2+} block of E224G are plotted for comparison. (B) The energy profile of the internal Ba^{2+} binding sites in the pore of the Kir2.1 channel. Sites marked with 'A' are the low-affinity binding sites in the cytoplasmic pore. Site B is the high-affinity binding site near T141.

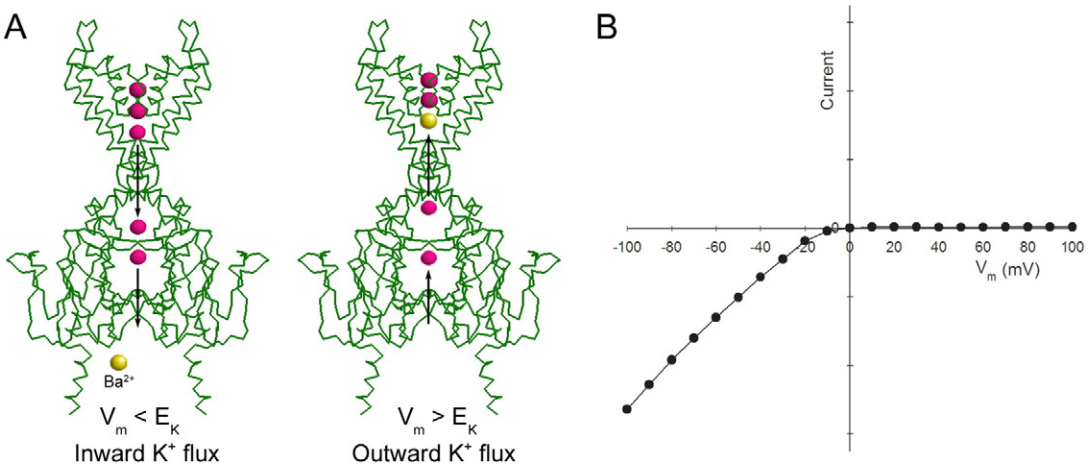

Fig. 11. (A) Schematic model of flux-dependent block of the Kir2.1 channel pore by internal Ba^{2+}. When the driving force ($V_m - E_K$) for K^+ ion conduction is negative, the K^+ flux is predominantly inward. The binding of K^+ ions on the cytoplasmic pore precludes the Ba^{2+} from encountering the high-affinity binding site. When the driving force is positive, the K^+ flux is predominantly outward. Ba^{2+} ions can be coupled to the K^+ efflux along the single-file, multi-ion long pore and encounter the binding site near T141 at the entrance of the selectivity filter. (B) I–V_m relationships of inward rectifier K^+ channels in symmetric K^+ concentrations ($E_K = 0$ mV) in the presence of internal blockers. Note that at voltages near but negative to E_K, the unidirectional K^+ efflux exists and flux-dependent block can occur, because backward transport is inevitable near the equilibrium.

Ba^{2+} block in this study, is also greatly influenced by the same driving force that influences K^+ ion conduction.

4.5. Model of the energy profile of the binding sites in the Kir2.1 channel for internal Ba^{2+} ions

We used the kinetic rate constants from this study to construct the model of the energy profile of the Ba^{2+} binding sites in the pore of Kir2.1 channels. The estimated binding rate constants or the unbinding rate constants at 0 mV could be used to calculate the energy barriers of the binding sites using the following relations:

$$k_{on} = C \exp\left(\frac{-\Delta G_{on}}{RT}\right) \tag{18}$$

and

$$k_{off} = C \exp\left(\frac{-\Delta G_{off}}{RT}\right). \tag{19}$$

The pre-exponential factor, C, is chosen as 10^9 s^{-1} because the free energy level is set to 0 at a 1 M ionic concentration, and the upper limit of the diffusion rate is approximately 10^9 M^{-1} s^{-1}. Hence, the value, 10^9, is a fair estimate of the natural attempting frequency. The energy profile at 0 mV is shown in Fig. 10B. The high-affinity binding site near T141 for the internal Ba^{2+} block is labeled 'B'. The electrical distance of this site from the internal side is approximately 20%. In a study of the block by internal TEA in the *Shaker* channel, the electrical distance was also 20% near the residue T441, which corresponds to T141 in the Kir2.1 channel [60]. The results suggest that 80% of the transmembrane potential drops in the region of selectivity filter [60,61]. The double mutant T141A–S165L has been shown to abolish external Rb^+ and Cs^+ block of inward K + current in the Kir2.1 channel and to permit Cs^+ to permeate as conduction ions [48], indicating that the high-affinity Ba^{2+} binding site near T141 and S165 may also play a key role in the K^+ permeation mechanism under physiological conditions. The sites labeled 'A' are the low-affinity ion binding sites in the cytoplasmic pore; the apparent dissociation constant is estimated to be in the millimolar range because 3 mM internal Ba^{2+} blocks only approximately 30% of the inward current at −100 mV. The low-affinity ion binding sites in the cytoplasmic pore are essential for the flux-coupling effect.

4.6. Implications of the Ba^{2+} block studies for the inward rectification under physiological conditions

One of the major contributions of this study is that we propose the mechanism of the inward rectification of internal Ba^{2+} block in the Kir2.1 channel. The steep voltage dependence of the block near E_K is caused by the flux-dependent block; thus, the block is dependent on the driving force for K^+ flux. In physiological conditions, the inward rectification of the Kir2.1 channel is caused by intracellular Mg^{2+} and polyamines. Some of the interpretation from our Ba^{2+} block study may be applied to studies of Mg^{2+} and polyamines. As a single-file long pore, the cytoplasmic pore provides an environment for the flux-coupling effect between K^+ ions and blocking ions. Although the binding sites for Ba^{2+}, Mg^{2+}, and polyamines may be different, the encounter frequency of the blockers should be coupled with the K^+ flux as long as there is a multi-ion, single-file region between the binding site and the intracellular entrance of the pore.

However, we have to keep in mind that there are differences in the mechanisms of inward rectification caused by Ba^{2+}, Mg^{2+} and polyamines. As shown in Fig. 1, in cell-attached configuration, the recovery rate is very fast when the voltage is stepped back to −100 mV from the steady-state block of outward currents at positive voltages. There are several mechanisms that underlie this phenomenon and it is significant in several aspects. In inside-out recordings, 1 mM internal Mg^{2+} cannot completely block the outward currents; 10% to 20% of steady-state currents remain in the presence of 1 mM internal Mg^{2+} [15]. The Mg^{2+} ion does not seem to have a high-affinity binding site like the Ba^{2+} ion has. During the steady-state block of outward currents, the Mg^{2+} might be steadily pushed by the outward K^+ ion flux and be locked within the pore. When the voltage is stepped back to −100 mV, the Mg^{2+} might be pushed back rapidly by the inward K^+ ion flux. Therefore, both the k_{on} and the k_{off} values in the block by internal Mg^{2+} may be subject to the K^+ flux coupling. Moreover, internal Mg^{2+} has been shown to induce discrete subconductance levels [62]; therefore, Mg^{2+}-induced gating has also been proposed. However, even with respect to the gating mechanism, if a Mg^{2+} ion has to move across the multi-ion, single-file region to reach the receptor site to induce the gating, the encounter frequency near E_K is still flux-dependent.

The inward rectification caused by intracellular spermine requires careful interpretation. In addition to the mechanism of flux-dependent pore block, when spermine molecules bind to the ring formed by the negative charge residues near E224, the effects of surface charge

screening could contribute significantly to the inward rectification by weakening the ion-concentrating ability at the internal vestibule [38] and by inducing a gating change in the Kir2.1 channel [13]. The K_d values for the inhibition by intracellular spermine have been shown to have two components: the first K_d was only ~1 nM and accounted for nearly 80% of the inhibition, and the second K_d was 0.6 μM, accounting for the remaining 20% of the inhibition [15]. The sensitive component of the inhibition suggests that some spermine molecules may constantly bind somewhere on the internal vestibule of Kir2.1 channels even in the presence of low concentrations of intracellular spermine. These molecules may cause inward rectification by inducing a flux-dependent gating mechanism. Hence, in inside-out recordings, when the voltage was stepped back to −100 mV from the steady-state inhibition of outward currents, the inward K^+ ion flux just pushed the flux-dependent barrier or gate to allow the inward currents. During this process, the spermine might still bind to the channel; therefore, the apparent recovery rate could be within milliseconds, whereas the K_d was only ~1 nM.

From the discussion above, we are aware that our studies here have focused on the pore-block mechanism by intracellular Ba^{2+} in the E224G mutant. The fast inhibition mechanism of internal Ba^{2+} in the wild-type Kir2.1 channels, which we have largely not addressed in this study, may also be an important component of the mechanisms of inward rectification. The inward rectification caused by Mg^{2+} and polyamines is complex in physiological conditions. Nevertheless, our study emphasizes the importance of the role of the multi-ion, single-file cytoplasmic pore in the flux-coupling effect, which is essential for the flux-dependent block by various intracellular blocking ions. The cytoplasmic pore is also essential for the flux-dependent gating of the K^+ flux in this channel and for the gating regulated by intracellular biochemical signals, e.g., the regulation by PIP_2 [27,52].

The relations between outward currents and the membrane potential in the Kir channels have great physiological significance. For example, in heart muscle cells, inward rectifier K^+ channels regulate the resting membrane potential and play interesting roles in shaping action potentials. The I–V_m relations of the outward currents have a positive-slope phase from E_K (near −90 mV) to −70 mV and have a negative-slope phase from −70 mV to −40 mV [63]. Kir channels function mainly during subthreshold depolarization and repolarization. The macroscopic conductance of Kir channels is low during the plateau phase of the action potential. Cardiac myocytes spend the majority of the time in depolarized states; in this period, the Kir channels are mostly shut due to the flux-dependent blockage of intracellular blocking ions. Evolution has equipped Kir channels with an efficient mechanism for harnessing the thermodynamic driving force for K^+ flux. This mechanism does not require a large spatial rearrangement of the channel protein structure, as occurs in voltage-dependent K^+ channels, but enables regulation of the blocking and gating actions and influences the excitability of the cells.

5. Conclusions

We present a novel model to elucidate the biophysical mechanisms underlying the strong inward rectification in Kir channels, based on studies of internal Ba^{2+}-mediated blockage in cloned Kir2.1 channels. The kinetic studies performed in different ionic and voltage conditions clearly demonstrated that the steep "voltage dependence" near the equilibrium potential actually results from the flux-coupling effect of the conducting K^+ ions on the blocking ion. The encounter frequency of the internal Ba^{2+} with the high-affinity binding site near T141 is strongly coupled with the K^+ flux along the single-file, multi-ion cytoplasmic long pore of Kir channels (Fig. 11A), which leads to steep changes of the binding rate near the equilibrium potential because the direction and magnitude of the unidirectional K^+ flux changes dramatically when the transmembrane voltages changes near E_K. The "driving force"-dependence block, and thus the flux-dependent block, can be demonstrated even in the presence of the concentration gradient alone, when there is no voltage difference across the membrane, as well as in the more general condition when the driving force is the electrochemical potential difference across the membrane.

Supplementary data to this article can be found online at http://dx.doi.org/10.1016/j.bpc.2015.04.003.

Acknowledgments

The authors thank Dr. Ru-Chi Shieh and her lab members for technical assistance and helpful discussion. C.P. Hsieh was a recipient of the M.D./Ph.D. predoctoral fellowship from the National Health Research Institute, Taiwan. This study was supported by grants from the Far Eastern Memorial Hospital (FEMH-2015-D-050) and from the Ministry of Science and Technology, Taiwan (NSC 95-2320-B-002-064-MY3).

References

[1] B. Hille, Ion Channels of Excitable Membranes, Sinauer, Sunderland, MA, 2001.
[2] Z. Lu, Mechanism of rectification in inward-rectifier K^+ channels, Annu. Rev. Physiol. 66 (2004) 103–129.
[3] C.G. Nichols, A.N. Lopatin, Inward rectifier potassium channels, Annu. Rev. Physiol. 59 (1997) 171–191.
[4] H. Matsuda, A. Saigusa, H. Irisawa, Ohmic conductance through the inwardly rectifying K channel and blocking by internal Mg^{2+}, Nature 325 (1987) 156–159.
[5] C.A. Vandenberg, Inward rectification of a potassium channel in cardiac ventricular cells depends on internal magnesium ions, Proc. Natl. Acad. Sci. U. S. A. 84 (1987) 2560–2564.
[6] D. Guo, Z. Lu, Mechanism of IRK1 channel block by intracellular polyamines, J. Gen. Physiol. 115 (2000) 799–814.
[7] A.N. Lopatin, E.N. Makhina, C.G. Nichols, Potassium channel block by cytoplasmic polyamines as the mechanism of intrinsic rectification, Nature 372 (1994) 366–369.
[8] A.M. Woodhull, Ionic blockage of sodium channels in nerve, J. Gen. Physiol. 61 (1973) 687–708.
[9] M. Spassova, Z. Lu, Coupled ion movement underlies rectification in an inward-rectifier K^+ channel, J. Gen. Physiol. 112 (1998) 211–221.
[10] D. Guo, Z. Lu, Interaction mechanisms between polyamines and IRK1 inward rectifier K^+ channels, J. Gen. Physiol. 122 (2003) 485–500.
[11] K. Ishihara, D.H. Yan, Low-affinity spermine block mediating outward currents through Kir2.1 and Kir2.2 inward rectifier potassium channels, J. Physiol. 583 (2007) 891–908.
[12] T.A. Liu, H.K. Chang, R.C. Shieh, Revisiting inward rectification: K ions permeate through Kir2.1 channels during high-affinity block by spermidine, J. Gen. Physiol. 139 (2012) 245–259.
[13] H.K. Chang, S.H. Yeh, R.C. Shieh, Charges in the cytoplasmic pore control intrinsic inward rectification and single-channel properties in kir1.1 and kir2.1 channels, J. Membr. Biol. 215 (2007) 181–193.
[14] Y. Kubo, T.J. Baldwin, Y.N. Jan, L.Y. Jan, Primary structure and functional expression of a mouse inward rectifier potassium channel, Nature 362 (1993) 127–133.
[15] J. Yang, Y.N. Jan, L.Y. Jan, Control of rectification and permeation by residues in two distinct domains in an inward rectifier K^+ channel, Neuron 14 (1995) 1047–1054.
[16] N. Alagem, M. Dvir, E. Reuveny, Mechanism of Ba^{2+} block of a mouse inwardly rectifying K^+ channel: differential contribution by two discrete residues, J. Physiol. Lond. 534 (2001) 381–393.
[17] F.C. Chatelain, N. Alagem, Q. Xu, R. Pancaroglu, E. Reuveny, D.L. Minor Jr., The pore helix dipole has a minor role in inward rectifier channel function, Neuron 47 (2005) 833–843.
[18] Y. Murata, Y. Fujiwara, Y. Kubo, Identification of a site involved in the block by extracellular Mg^{2+} and Ba^{2+} as well as permeation of K^+ in the Kir2.1 K^+ channel, J. Physiol. Lond. 544 (2002) 665–677.
[19] J. Neyton, C. Miller, Discrete Ba^{2+} block as a probe of ion occupancy and pore structure in the high-conductance Ca^{2+}-activated K^+ channel, J. Gen. Physiol. 92 (1988) 569–586.
[20] R.C. Shieh, J.C. Chang, J. Arreola, Interaction of Ba^{2+} with the pores of the cloned inward rectifier K^+ channels Kir2.1 expressed in *Xenopus* oocytes, Biophys. J. 75 (1998) 2313–2322.
[21] G.A. Thompson, M.L. Leyland, I. Ashmole, P.R. Stanfield, Residues in H5 and M2 of murine Kir2.1 regulate Ba^{2+} block, J. Physiol. Lond. 526 (2000) 115P.
[22] S.B. Hansen, X. Tao, R. MacKinnon, Structural basis of PIP2 activation of the classical inward rectifier K^+ channel Kir2.2, Nature 477 (2011) 495–498.
[23] M. Nishida, M. Cadene, B.T. Chait, R. MacKinnon, Crystal structure of a Kir3.1-prokaryotic Kir channel chimera, EMBO J. 26 (2007) 4005–4015.
[24] M. Nishida, R. MacKinnon, Structural basis of inward rectification: cytoplasmic pore of the G protein-gated inward rectifier GIRK1 at 1.8 A resolution, Cell 111 (2002) 957–965.
[25] S. Pegan, C. Arrabit, P.A. Slesinger, S. Choe, Andersen's syndrome mutation effects on the structure and assembly of the cytoplasmic domains of Kir2.1, Biochemistry 45 (2006) 8599–8606.
[26] X. Tao, J.L. Avalos, J. Chen, R. MacKinnon, Crystal structure of the eukaryotic strong inward-rectifier K^+ channel Kir2.2 at 3.1 A resolution, Science 326 (2009) 1668–1674.

[27] C.L. Huang, S. Feng, D.W. Hilgemann, Direct activation of inward rectifier potassium channels by PIP_2 and its stabilization by Gβγ, Nature 391 (1998) 803–806.
[28] T. Rohacs, C. Lopes, T. Mirshahi, T. Jin, H. Zhang, D.E. Logothetis, Assaying phosphatidylinositol bisphosphate regulation of potassium channels, Methods Enzymol. 345 (2002) 71–92.
[29] L.H. Xie, S.A. John, B. Ribalet, J.N. Weiss, Long polyamines act as cofactors in PIP2 activation of inward rectifier potassium (Kir2.1) channels, J. Gen. Physiol. 126 (2005) 541–549.
[30] W.M. Weber, K.M. Liebold, F.W. Reifarth, U. Uhr, W. Clauss, Influence of extracellular Ca^{2+} on endogenous Cl^- channels in *Xenopus* oocytes, Pflugers Arch. 429 (1995) 820–824.
[31] M.M. White, M. Aylwin, Niflumic and flufenamic acids are potent reversible blockers of Ca^{2+}-activated Cl^- channels in *Xenopus* oocytes, Mol. Pharmacol. 37 (1990) 720–724.
[32] D. Guo, Z. Lu, Pore block versus intrinsic gating in the mechanism of inward rectification in strongly rectifying IRK1 channels, J. Gen. Physiol. 116 (2000) 561–568.
[33] R.C. Shieh, S.A. John, J.K. Lee, J.N. Weiss, Inward rectification of the IRK1 channel expressed in *Xenopus* oocytes: effects of intracellular pH reveal an intrinsic gating mechanism, J. Physiol. Lond. 494 (Pt 2) (1996) 363–376.
[34] B. Hille, W. Schwarz, Potassium channels as multi-ion single-file pores, J. Gen. Physiol. 72 (1978) 409–442.
[35] C.M. Armstrong, Interaction of tetraethylammonium ion derivatives with the potassium channels of giant axons, J. Gen. Physiol. 58 (1971) 413–437.
[36] S.-H. Yeh, H.-K. Chang, R.-C. Shieh, Electrostatics in the cytoplasmic pore produce intrinsic inward rectification in Kir2.1 channels, J. Gen. Physiol. 126 (2005) 551–562.
[37] M. Holmgren, P.L. Smith, G. Yellen, Trapping of organic blockers by closing of voltage-dependent K^+ channels: evidence for a trap door mechanism of activation gating, J. Gen. Physiol. 109 (1997) 527–535.
[38] L.H. Xie, S.A. John, J.N. Weiss, Spermine block of the strong inward rectifier potassium channel Kir2.1: dual roles of surface charge screening and pore block, The, J. Gen. Physiol. 120 (2002) 53–66.
[39] A.L. Hodgkin, R.D. Keynes, The potassium permeability of a giant nerve fibre, J. Physiol. Lond. 128 (1955) 61–88.
[40] H.H. Ussing, The distinction by means of tracers between active transport and diffusion. The transfer of iodide across the isolated frog skin, Acta Physiol. Scand. 19 (1949) 43–56.
[41] A. Katchalsky, P.F. Curran, Nonequilibrium Thermodynamics in Biophysics, Harvard University Press, Cambridge, 1965.
[42] C.J. Abrams, N.W. Davies, P.A. Shelton, P.R. Stanfield, The role of a single aspartate residue in ionic selectivity and block of a murine inward rectifier K^+ channel Kir2.1, J. Physiol. 493 (Pt 3) (1996) 643–649.
[43] B. Fakler, U. Brandle, C. Bond, E. Glowatzki, C. Konig, J.P. Adelman, H.P. Zenner, J.P. Ruppersberg, A structural determinant of differential sensitivity of cloned inward rectifier K^+ channels to intracellular spermine, FEBS Lett. 356 (1994) 199–203.
[44] P.R. Stanfield, N.W. Davies, P.A. Shelton, M.J. Sutcliffe, I.A. Khan, W.J. Brammar, E.C. Conley, A single aspartate residue is involved in both intrinsic gating and blockage by Mg^{2+} of the inward rectifier, IRK1, J. Physiol. 478 (Pt 1) (1994) 1–6.
[45] B.A. Wible, M. Taglialatela, E. Ficker, A.M. Brown, Gating of inwardly rectifying K^+ channels localized to a single negatively charged residue, Nature 371 (1994) 246–249.
[46] T. Lu, L. Wu, J. Xiao, J. Yang, Permeant ion-dependent changes in gating of Kir2.1 inward rectifier potassium channels, J. Gen. Physiol. 118 (2001) 509–522.
[47] Y. Fujiwara, Y. Kubo, Ser165 in the second transmembrane region of the Kir2.1 channel determines its susceptibility to blockade by intracellular Mg^{2+}, J. Gen. Physiol. 120 (2002) 677–693.
[48] G.A. Thompson, M.L. Leyland, I. Ashmole, M.J. Sutcliffe, P.R. Stanfield, Residues beyond the selectivity filter of the K^+ channel Kir2.1 regulate permeation and block by external Rb^+ and Cs^+, J. Physiol. Lond. 526 (2000) 231–240.
[49] B.A. Yi, Y.F. Lin, Y.N. Jan, L.Y. Jan, Yeast screen for constitutively active mutant G protein-activated potassium channels, Neuron 29 (2001) 657–667.
[50] F. Kiefer, K. Arnold, M. Kunzli, L. Bordoli, T. Schwede, The SWISS-MODEL Repository and associated resources, Nucleic Acids Res. 37 (2009) D387–D392.
[51] Y.X. Jiang, R. MacKinnon, The barium site in a potassium channel by X-ray crystallography, J. Gen. Physiol. 115 (2000) 269–272.
[52] S. Pegan, C. Arrabit, W. Zhou, W. Kwiatkowski, A. Collins, P.A. Slesinger, S. Choe, Cytoplasmic domain structures of Kir2.1 and Kir3.1 show sites for modulating gating and rectification, Nat. Neurosci. 8 (2005) 279–287.
[53] C.C. Kuo, P. Hess, Characterization of the high-affinity Ca^{2+} binding sites in the L-type Ca^{2+} channel pore in rat phaeochromocytoma cells, J. Physiol. Lond. 466 (1993) 657–682.
[54] C.C. Kuo, P. Hess, Ion permeation through the L-type Ca^{2+} channel in rat phaeochromocytoma cells: two sets of ion binding sites in the pore, J. Physiol. Lond. 466 (1993) 629–655.
[55] C.C. Kuo, T.J. Lin, C.P. Hsieh, Effect of Na^+ flow on Cd^{2+} block of tetrodotoxin-resistant Na^+ channels, J. Gen. Physiol. 120 (2002) 159–172.
[56] A. Inanobe, T. Matsuura, A. Nakagawa, Y. Kurachi, Structural diversity in the cytoplasmic region of G protein-gated inward rectifier K^+ channels, Channels 1 (2007) 39–45.
[57] C.P. Hsieh, Interpretation of the Ussing flux ratio from the fluctuation theorem, Biophys. Chem. 139 (2009) 57–62.
[58] R.P. Feynman, R.B. Leighton, M. Sands, The Feynman Lectures on Physics, Addison-Wesley, Reading, 1963.
[59] P.A. Skordos, W.H. Zurek, Maxwell's demon, rectifiers, and the second law: computer simulation of Smoluchowski's trapdoor, Am. J. Phys. 60 (1992) 876–882.
[60] G. Yellen, M.E. Jurman, T. Abramson, R. MacKinnon, Mutations affecting internal TEA blockade identify the probable pore-forming region of a K^+ channel, Science 251 (1991) 939–942.
[61] D.A. Doyle, J. Morais Cabral, R.A. Pfuetzner, A. Kuo, J.M. Gulbis, S.L. Cohen, B.T. Chait, R. MacKinnon, The structure of the potassium channel: molecular basis of K+ conduction and selectivity, Science 280 (1998) 69–77.
[62] H. Matsuda, Open-state substructure of inwardly rectifying potassium channels revealed by magnesium block in guinea-pig heart cells, J. Physiol. Lond. 397 (1988) 237–258.
[63] M. Delmar, J. Ibarra, J. Davidenko, P. Lorente, J. Jalife, Dynamics of the background outward current of single guinea pig ventricular myocytes. Ionic mechanisms of hysteresis in cardiac cells, Circ. Res. 69 (1991) 1316–1326.